Journal of Medicinal Chemistry

pubs.acs.org/jmc

Drug Annotation

Design, Synthesis, and Characterization of TNP-2198, a Dual-Targeted Rifamycin-Nitroimidazole Conjugate with Potent Activity against Microaerophilic and Anaerobic Bacterial Pathogens

Zhenkun Ma,* Shijie He, Ying Yuan, Zhijun Zhuang, Yu Liu, Huan Wang, Jing Chen, Xiangyi Xu, Charles Ding, Vadim Molodtsov, Wei Lin, Gregory T. Robertson, William J. Weiss, Mark Pulse, Phung Nguyen, Leonard Duncan, Timothy Doyle, Richard H. Ebright, and Anthony Simon Lynch

Cite This: *J. Med. Chem.* 2022, 65, 4481−4495

Read Online

ACCESS | Metrics & More | Article Recommendations | Supporting Information

ABSTRACT: TNP-2198, a stable conjugate of a rifamycin pharmacophore and a nitroimidazole pharmacophore, has been designed, synthesized, and evaluated as a novel dual-targeted antibacterial agent for the treatment of microaerophilic and anaerobic bacterial infections. TNP-2198 exhibits greater activity than a 1:1 molar mixture of the parent drugs and exhibits activity against strains resistant to both rifamycins and nitroimidazoles. A crystal structure of TNP-2198 bound to a *Mycobacterium tuberculosis* RNA polymerase transcription initiation complex reveals that the rifamycin portion of TNP-2198 binds to the rifamycin binding site on RNAP and the nitroimidazole portion of TNP-2198 interacts directly with the DNA template-strand in the RNAP active-center cleft, forming a hydrogen bond with a base of the DNA template strand. TNP-2198 is currently in Phase 2 clinical development for the treatment of *Helicobacter pylori* infection, *Clostridioides difficile* infection, and bacterial vaginosis.

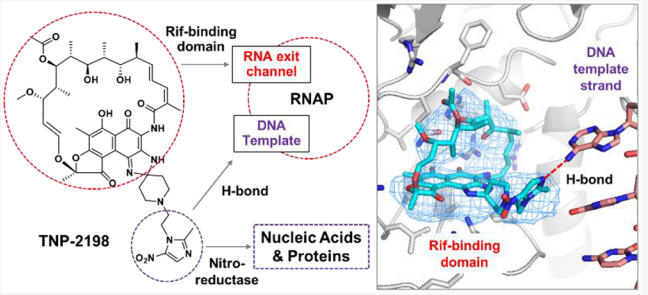

INTRODUCTION

The relentless emergence and iteration of antimicrobial resistance (AMR) and its epidemiological spread dictates the continuous development of new antimicrobial agents and, perhaps more important, novel approaches to alter the trajectory of current resistance trends in key pathogens.[1−3] Current drug development efforts in this area are mainly focused on the identification of new modalities in existing approved antibiotic classes for the treatment of multidrug resistant Gram-positive and Gram-negative infections, such as methicillin-resistant *Staphylococcus aureus* (MRSA), carbapenem-resistant Enterobacteriaceae (CRE), and carbapenem-resistant *Acinetobacter baumannii* (CRAB). Only limited efforts have been devoted to the development of new therapies for the treatment of anaerobic and microaerophilic bacterial infections, such as those caused by *Helicobacter pylori*, *Clostridioides difficile* and *Gardnerella vaginosis*, despite a growing unmet need in this area.[4−6]

Contemporary estimates of incidences of *H. pylori* infection in humans range from 28% to 84% in different geographies and subpopulations thereof.[7] Symptomatic complications range from mild to severe diseases encompassing gastritis, gastric and duodenal ulcers, gastric cancer, and gastric mucosa-associated lymphoid tissue (MALT) lymphoma, underlying the identification of *H. pylori* as a key World Health Organization priority pathogen and carcinogen.[8] Current recommended first-line treatment for diagnosed, symptomatic diseases include the use of proton pump inhibitors in combination with at least two antibiotics over 7−14 days of therapy.[7] Failure of patients on recommended first-line treatment regimens dictates the use of recommended second-line regimens or empiric therapy.[7,9,10] Due to high-level resistance to available antibiotics in China and many other regions in the world, individualized bismuth-containing quadruple therapy has been recommended for the management of *H. pylori* infection. Current trends in contemporary antibiotic resistance in *H. pylori* do not hold long-term promise for the use of currently approved antibiotics.[11]

The incidence and severity of *Clostridioides difficile*-associated diarrhea (CDAD) in primary disease has increased over the past decade, including reports of metronidazole treatment failure.[12] Relapse of primary CDAD dictates the use of second line or alternative therapies including the use of

Received: November 30, 2021
Published: February 17, 2022

https://doi.org/10.1021/acs.jmedchem.1c02045
J. Med. Chem. 2022, 65, 4481−4495

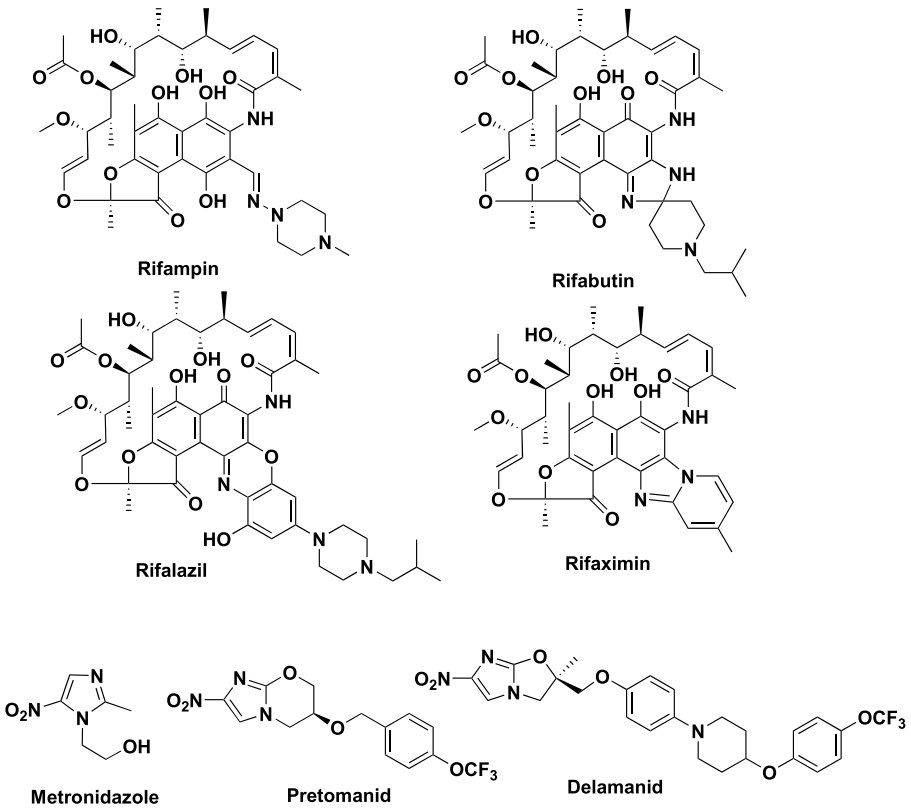

Figure 1. Structures of representative rifamycins (first and second rows) and nitroimidazoles (third row) antibacterial agents.

intravenously administered antibodies.[13] In the treatment of primary or secondary/relapse CDAD there is a clear unmet medical need to develop new agents.

Bacterial vaginosis is associated with vaginal inflammation caused by the overgrowth of pathogenic bacteria in the vaginal tract, upsetting the vaginal natural microbiome. Bacterial vaginosis most frequently affects women in their reproductive years, but can affect women of any age and can predispose women to sexually transmitted infections including HIV. Recurrent bacterial vaginosis requires prolonged treatments to return the vaginal microbiome to a normal *Lactobacillus*-dominated environment. Current treatment recommendations encompass the administration of metronidazole orally or intravaginally for 5−7 days.[14]

In previous publications, we have described TNP-2092—a stable conjugate of a rifamycin pharmacophore and a quinolizinone (a bioisostere of a quinolone) pharmacophore—as a triple-targeted antibacterial agent with potent activity against bacterial biofilm-associated infections, including those caused by MRSA.[15−19] TNP-2092 exerts its bactericidal activity by inhibiting three essential, clinically validated antibacterial targets: inhibiting RNA polymerase (RNAP) through its rifamycin pharmacophore and inhibiting DNA gyrase and DNA topoisomerase IV through its quinolizinone pharmacophore. TNP-2092 is effective against rifamycin-resistant strains (exerting activity against rifamycin-resistant strains through its quinolizinone pharmacophore) and is effective against fluoroquinolone-resistant strains (exerting activity through its rifamycin pharmacophore). TNP-2092 is refractory to identified efflux mechanisms and exhibits a low frequency of development of intrinsic target-based resistance.[15−17]

The strategy of stably conjugating two different antimicrobial pharmacophores in a single molecular entity, as exemplified by TNP-2092,[15] provides important advantages over the alternative strategy of combining currently approved antimicrobial agents into combination regimens, including matched pharmacokinetics, matched tissue distribution, and as exemplified herein, the potential for mechanism-based synergy.[20,21]

Rifamycins are an important class of antibacterial agents[22,23] exhibiting antibacterial activity by inhibiting bacterial RNAP.[24−27] Rifamycins inhibit bacterial RNAP by binding to a site on bacterial RNAP (Rif binding pocket) located adjacent to the RNAP active center and preventing short, 2-3 nucleotide RNA products from being extended to yield longer RNA transcripts. Drugs in the rifamycin class, including rifampin (Rif), rifapentine, rifabutin, rifaximin (Figure 1), have been approved for multiple antibacterial indications, including treatment of tuberculosis, for which they are first-line drugs, treatment of nontuberculous Mycobacterial infections, treatment of staphylococcal bone and joint infections, and treatment and prophylaxis of diarrhea and hepatic encephalopathy.[23] However, due to the relatively high frequency of development of intrinsic resistance, rifamycins generally are not used as monotherapeutic agents in the treatment of bacterial infections and instead are restricted to be used as components of multidrug combination regimens with the exception of rifaximin.

Nitroimidazoles are a family of antimicrobial agents used in the treatment of bacterial infections, trichomoniasis, amoebiasis, and giardiasis.[28,29] Nitroimidazoles exert antimicrobial activity through intracellular reduction to hydroxylamine-imidazoles or other reactive species, followed by covalent cross-linking with nucleic acids or proteins.[30] Currently

https://doi.org/10.1021/acs.jmedchem.1c02045
J. Med. Chem. 2022, 65, 4481−4495

marketed nitroimidazoles, including metronidazole, pretomanid, and delamanid (Figure 1), are approved for the treatment of microaerophilic and anaerobic eubacterial infections and for Mycobacterial diseases.[29,31]

Considering the clinical importance and validation of current agents within the rifamycin and nitroimidazole classes, a series of rifamycin-nitroimidazole conjugate molecules were designed, synthesized, and evaluated for the potential treatment of microaerophilic and anaerobic bacterial infections.

RESULTS AND DISCUSSION

Identification of TNP-2198. The design of rifamycin-nitroimidazole conjugate molecules was based on crystal structures of RNAP and RNAP-containing transcription initiation complexes bound to rifamycins[24,25,32,26,33−38] and on structure−activity relationships (SAR) for both the rifamycin and nitroimidazole drug classes.[24−26,15,38,39,37]

Crystal structures of RNAP and RNAP-containing transcription initiation complexes bound to rifamycins indicate that the rifamycin C3, C4, and C25 positions are adjacent to an open space between the RNAP Rif pocket and the RNAP active center and show that the attachment of substituents can be tolerated at these positions.[24,25,32,26,33−35,38,36,37] SAR for rifamycins confirms that the attachment of substituents, even relatively large substituents, can be tolerated at the rifamycin C3, C4, and C25 positions. These positions therefore were explored as preferred sites for the attachment of a second antibacterial pharmacophore to the rifamycin scaffold to yield bifunctional, dual-targeted antibacterial agents (Figure 2).[15]

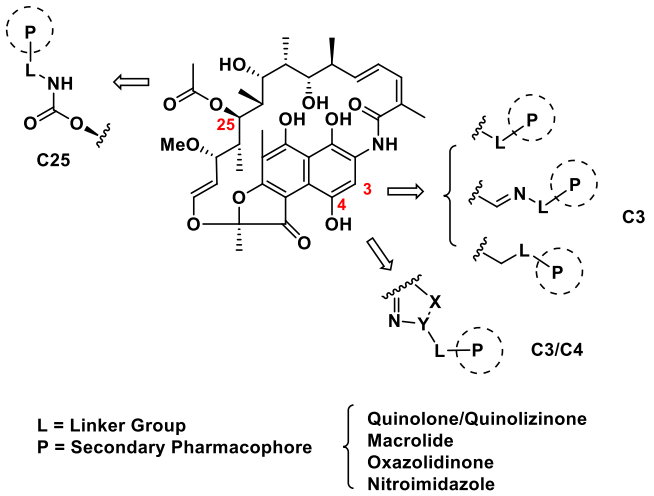

Figure 2. Rifamycin-based conjugate series explored. The C3, C4, and C25 positions of the rifamycin pharmacophore are highlighted in red. L, linker group; P, secondary pharmacophore.

A series of five rifamycin scaffold templates, based on marketed products and developmental drug candidates, were utilized to design the rifamycin-nitroimidazole conjugate molecules reported herein (Figure 3). Structures I, III, and V are based on the approved rifamycin drugs rifampin, rifabutin, and rifaximin, respectively. Structure IV is based on the rifamycin drug candidate, rifalazil. A series of four nitroimidazoles (A, B, C, and D) and one nitrothiazole (E) were utilized as the secondary pharmacophore (P). These structures are based on the commercialized products metronidazole, delamanid, pretomanid, and nitazoxanide, respectively. Various linker groups (L) were explored to link the rifamycin and the nitroimidazole/nitrothiazole pharmacophores. However, as a general principle, the linker groups explored were kept to a minimum in size to maintain the established PK/PD properties of the parental pharmacophores and therein the potential for oral bioavailability.

The minimum inhibitory concentrations (MICs) of representative rifamycin-nitroimidazole conjugates, as compared to rifamycin and nitroimidazole parent drugs, against the facultative anaerobe bacterium *S. aureus* (aerobically propagated), the microaerophilic bacterium *H. pylori*, and the obligate anaerobic bacterium *C. difficile* are summarized in Table 1. Overall, conjugate series derivatized from rifamycin structures III and IV provided the most promising overall activity against *H. pylori* and *C. difficile*. A variety of nitroimidazole/nitrothiazole groups and linker structures could be tolerated. It appeared that the antibacterial activities of the conjugate molecules were mainly driven by the rifamycin pharmacophore rather than the nitroimidazole functionality, as the MICs of the conjugate series were similar to that of the parenteral rifamycin agents.

Compounds **1**, **2**, **10**, **15**, and **17** were among the most potent conjugates (Figure 4). These compounds are different with regard to the rifamycin pharmacophore component, but all contain the same metronidazole pharmacophore fused by an ethylene linker. The MICs of these compounds against *H. pylori* ATCC 700392 and a rifamycin-resistant (*rpoB*$^{L525I,\ D530N}$) variant as well as *C. difficile* ATCC BAA 1382 and a rifamycin-resistant (*rpoB*^{Q489K}) variant are summarized in Table 2. These *rpoB* mutations result in a high level of resistance to rifamycins as exemplified by the high MICs of rifampin against these strains. The activity of the conjugate molecules against these *rpoB* variants represents the contribution of the nitroimidazole functionality as determined under the *in vitro* experimental conditions. With the exception of compound **17**, all compounds exhibited lower MICs against the *rpoB* mutant strains than rifampin and therein apparent dual functionality. Compound **10** appeared to be more potent than metronidazole against the *H. pylori rpoB* mutant and equally potent to metronidazole against the *C. difficile rpoB* mutant. Further evaluation of the rifamycin-nitroimidazole conjugate series identified compound **10** (TNP-2198) as a potential development candidate for the treatment of microaerophilic and anaerobic infections.

TNP-2198 Mode of Action: Dual-Targeted and Synergistic Antibacterial Activities. To elucidate further the activities of TNP-2198 against rifamycin-resistant and nitroimidazole-resistant mutants, a series *H. pylori* mutants were generated from the wild-type *H. pylori* ATCC 700392 strain by stepwise selection for resistance to Rif, to Mtz, or to both, and corresponding *rpoB* and *rdxA* (encoding the key oxygen-insensitive nitroreductase)[40,41] resistance determinants were sequenced to identify the sequence changes associated with resistance. The resulting strain set of *H. pylori* ATCC 700392 variants bearing Rif-resistant (*rpoB*^{D530V}, *rpoB*^{V149F}, *rpoB*^{L525I,G522D}, *rpoB*^{L525I,L544H}, and *rpoB*^{L525I,D530N}) and/or Mtz-resistant (*rdxA*^{R16S}, and *rdxA*^{E75S}) alleles were selected for further characterization (Table 3).

As expected, Rif and Rbt showed reduced effectiveness against the Rif-resistant strains CB1902, CB1903, CB1612, CB1613, and CB1614; metronidazole showed reduced effectiveness against the Mtz-resistant strain CB1573, and

https://doi.org/10.1021/acs.jmedchem.1c02045
J. Med. Chem. 2022, 65, 4481−4495

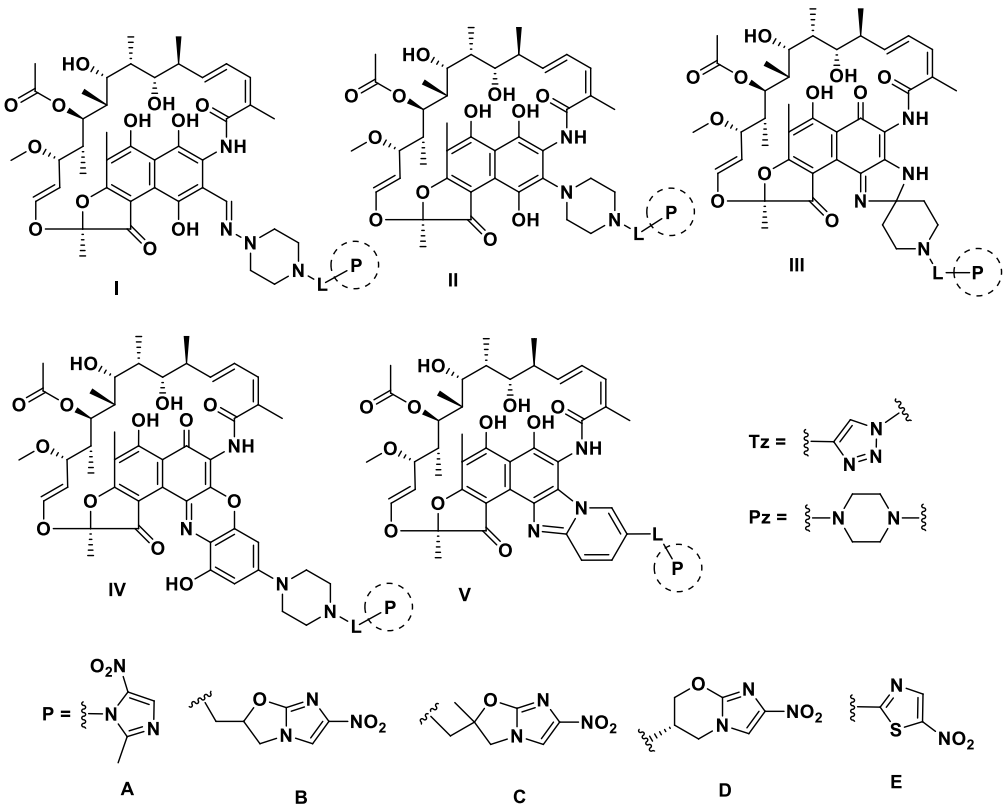

Figure 3. Structures of representative rifamycin-nitroimidazole conjugates.

Table 1. Structure–Activity Relationship of Representative Rifamycin-Nitroimidazole Conjugates against *S. aureus*, *C. difficile*, and *H. pylori*[a]

				MIC (μg/mL)		
compd	series	L	P	*S. aureus* ATCC 29213	*C. difficile* ATCC 9689	*H. pylori* ATCC 700392
1	I	$-CH_2CH_2-$	A	0.03	0.002	0.25
2	II	$-CH_2CH_2-$	A	<0.015	0.00025	0.06
3	II	$-CH_2$(*p*-Ph)O–	B	<0.004	NT	0.25
4	II	–	C	0.008	0.001	0.25
5	II	–(*p*-Ph)O–	C	0.015	0.03	1
6	II	–CO(*p*-Ph)O–	C	0.25	NT	4
7	II	$-COCH_2$Pz(*p*-Ph)O–	C	0.03	NT	2
8	II	$-CH_2$(*p*-Ph)CH_2O-	D	<0.008	0.008	0.5
9	II	$-COCH_2O-$	D	2	NT	4
10 (TNP-2198)	III	$-CH_2CH_2-$	A	0.015	0.0002	0.002
11	III	–	B	0.015	NT	0.06
12	III	–	C	0.03	NT	0.03
13	III	$-CH_2$(*p*-Ph)CH_2O-	D	0.03	0.001	0.03
14	III	$-CH_2CONH-$	E	NT	0.001	0.004
15	IV	$-CH_2CH_2-$	A	<0.03	0.002	0.004
16	IV	–(*p*-Ph)O–	C	<0.008	0.03	0.06
17	V	$-CH_2CH_2COPzCH_2CH_2-$	A	NT	0.004	1
	rifampin (Rif)			0.008	0.001	0.25
	rifabutin (Rbt)			0.03	0.0001	0.001
	rifalazil (Rfz)			0.004	0.001	0.002
	rifaximin (Rxm)			0.06	0.004	1
	metronidazole (Mtz)			>32	0.5	2
	pretomanid (Pre)			>32	16	2
	delamanid (Del)			>32	>16	2

[a]NT, not tested; *p*-Ph, *para*-phenylene; Pz, piperazine-1,4-diyl.

Rif, Rbt, and Mtz all showed reduced effectiveness against the Rif-resistant, Mtz-resistant strains CB1771 and CB1893.

TNP-2198 was more active than Rif and Rbt against Rif-resistant strains, consistent with the intended dual-targeted

https://doi.org/10.1021/acs.jmedchem.1c02045
J. Med. Chem. 2022, 65, 4481–4495

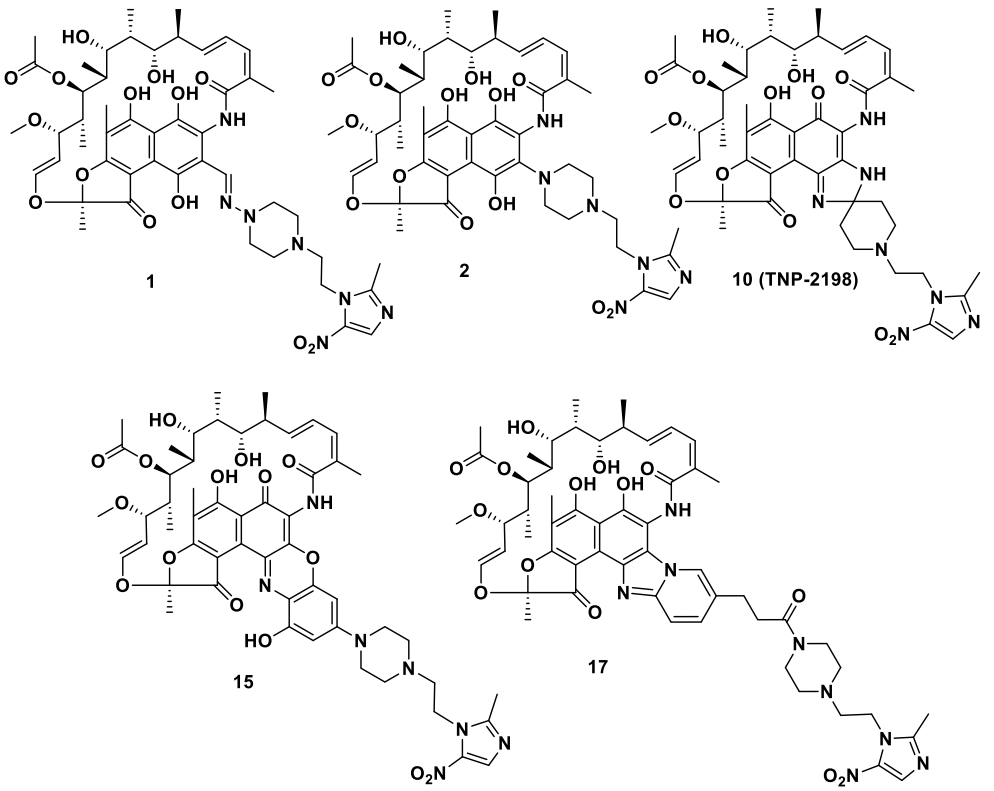

Figure 4. Structures of representative rifamycin-metronidazole conjugates.

Table 2. Structure−Activity Relationships of Representative Rifamycin-Metronidazole Conjugates against *C. difficile* and *H. pylori* Strains, Including Variants with Defined Rifamycin-Resistant (*rpoB*) Mutations[a]

	MIC (μg/mL)			
	H. pylori		*C. difficile*	
compd	ATCC 700392	Rif-R ($rpoB^{L525I,D530N}$)	ATCC BAA 1382	Rif-R ($rpoB^{Q489K}$)
1	0.25	2	0.0005	2
2	0.06	NT	0.00025	NT
10 (TNP-2198)	**0.004**	**0.5**	**0.00025**	**0.25**
15	0.004	0.5	0.001	2
17	1	>8	0.004	4
Mtz	2	2	0.25	0.25
Rif	0.25	>32	0.001	>8

[a]NT: not tested.

activity of TNP-2198, in which activity against Rif-resistant strains is provided by the nitroimidazole pharmacophore (strains CB1902, CB1903, CB1612, CB1613, and CB1614). TNP-2198 also was more active than Mtz against the Mtz-resistant strain, consistent with the intended dual-targeted activity of TNP-2198, in which activity against the Mtz-resistant strain is provided by the rifamycin pharmacophore (strain CB1573).

Unexpectedly, TNP-2198 not only was more active than Rif and Rbt against Rif-resistant strains but also was 4- to 125-fold more active than Mtz against Rif-resistant strains. Also unexpectedly, TNP-2198 was 32- to 64-fold more active than Rif, Rbt, or Mtz against dual Rif-resistant, Mtz-resistant strains (CB1771 and CB1893). These unexpected results indicate that conjugation of the rifamycin and nitroimidazole pharmacophores in TNP-2198 may exhibit a synergistic activity, above and beyond the intended dual-targeted activity.

To test the hypothesis that the rifamycin and nitroimidazole pharmacophores of TNP-2198 exhibit a synergistic activity, we next compared the effects of 1:1 molar combinations of Rif and Mtz and of Rbt and Mtz to that of TNP-2198. Consistent with the hypothesis, TNP-2198 was 4- to 128-fold more active against the Rif-resistant strains (strains CB1902, CB1903 and

Table 3. MICs (μg/mL) of TNP-2198 against Rif-Resistant, Mtz-Resistant, and Rif-Resistant, Mtz-Resistant *H. pylori* Strains

strain	description	Rif	Rbt	Mtz	Rif + Mtz (1:1 molar ratio)	Rbt + Mtz (1:1 molar ratio)	TNP-2198
ATCC 700392	wild-type	0.5	≤0.002	2	0.5	≤0.002	≤0.002
CB1573	Mtz-R ($rdxA^{R16S}$)	0.5	≤0.002	32	0.25	≤0.002	≤0.002
CB1902	Rif-R ($rpoB^{V149F}$)	>32	16	2	8	2	0.5
CB1903	Rif-R ($rpoB^{D530V}$)	>32	16	2	16	1	0.125
CB1614	Rif-R ($rpoB^{L525I,\ D530N}$)	>32	16	2	8	2	0.125
CB1771	Mtz-R/Rif-R ($rpoB^{L525I,\ D530N}/rdxA^{E7Stop}$)	>32	16	32	>32	16	0.5
CB1893	Mtz-R/Rif-R ($rpoB^{L525I,\ D530N}/rdxA^{R16S}$)	>32	16	32	>32	16	0.5

https://doi.org/10.1021/acs.jmedchem.1c02045
J. Med. Chem. 2022, 65, 4481−4495

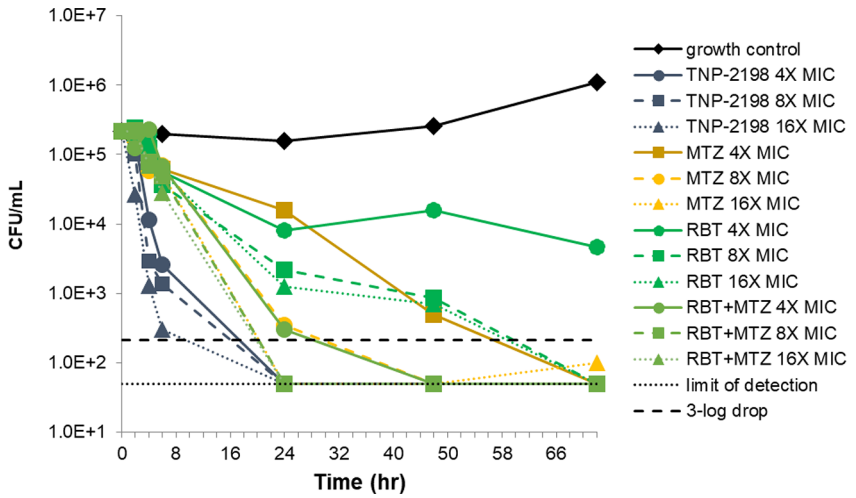

Figure 5. Bactericidal kinetics of TNP-2198, Rbt, and Mtz and 1:1 molar combination of Rbt and Mtz against *H. pylori* ATCC 700824.

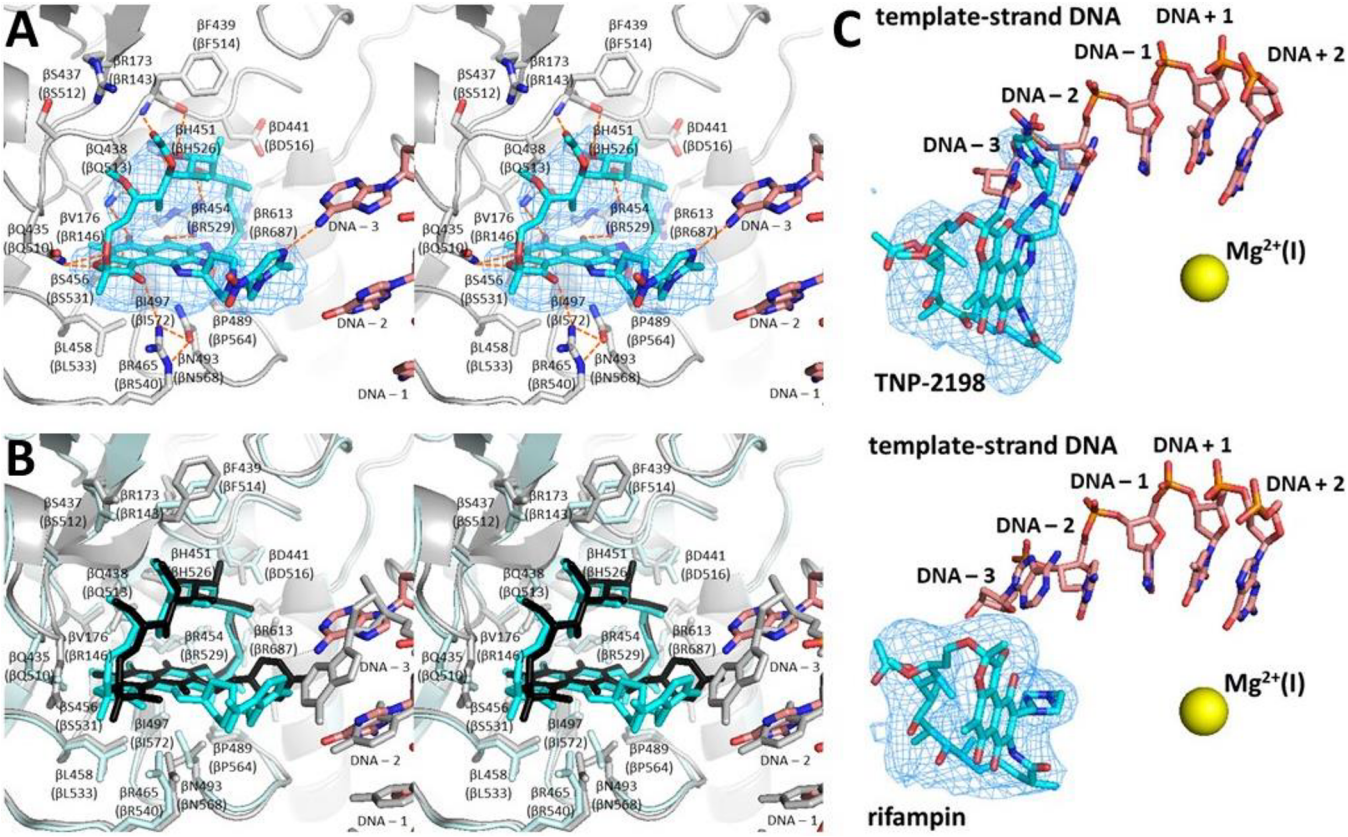

Figure 6. Structure of *M. tuberculosis* RNAP-promoter open complex bound to TNP-2198. (A) Stereodiagram of interactions between TNP-2198, RNAP, and promoter template-strand single-stranded DNA. Blue mesh, $2F_o - F_c$ electron density for TNP-2198, contoured at 1.2 σ; cyan, red, and blue sticks, carbon, oxygen, and nitrogen atoms, respectively, of TNP-2198; gray ribbon, RNAP backbone; gray, red, and blue sticks, carbon, oxygen, and nitrogen atoms of RNAP side chains that contact TNP-2198; pink, red, and blue sticks, carbon, oxygen, and nitrogen atoms of DNA; red dashes, hydrogen-bonds. (B) Stereodiagram showing superimposition of structure of *M. tuberculosis* RNAP-promoter open complex bound to TNP-2198 (cyan for TNP-2198; light cyan for RNAP) on structure of *M. tuberculosis* RNAP-promoter open complex bound to Rif (black for Rif, gray for RNAP; PDB 5UHB.[26] (C) Relationship of TNP-2198 (top) and Rif (bottom) to promoter template-strand single-stranded DNA and RNAP-active-center catalytic Mg^{2+} ion in structures of (B). Yellow sphere, RNAP-active-center Mg^{2+}. Other colors as in (A).

CB1614), 1- to 125-fold more active against the Mtz-resistant strain (CB1573), and 1- to 125-fold more active against the Rif-resistant, Mtz-resistant strains (CB1771 and CB1893) than the 1:1 molar combination of the parent drugs. Taken together, the results in Table 3 indicated that the rifamycin and the nitroimidazole pharmacophores of TNP-2198 exhibited the intended dual-targeted activity and also exhibited an unexpected synergistic activity.

In an analogous analysis for *C. difficile*, a series of *C. difficile* mutants was generated from the wild-type ATCC BAA1382 strain by stepwise selection for resistance to Rif, to the fluoroquinolone ciprofloxacin (Cipro), or to both, and *rpoB*

https://doi.org/10.1021/acs.jmedchem.1c02045
J. Med. Chem. 2022, 65, 4481−4495

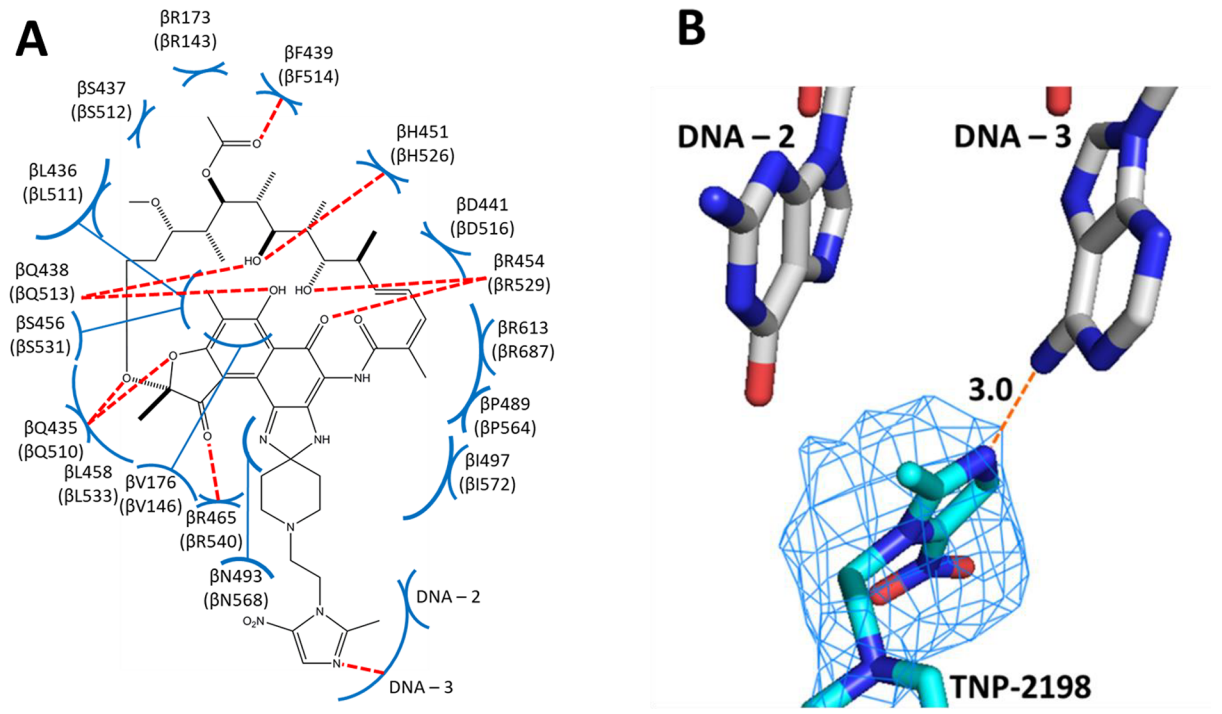

Figure 7. Structure of *M. tuberculosis* RNAP-promoter open complex bound to TNP-2198. (A) Schematic summary of interactions (residues numbered as in *M. tuberculosis* RNAP and, in parentheses, as in *Escherichia coli* RNAP). Red dashed lines, hydrogen-bonds; blue arcs and blue lines, van der Waals interactions. (B) Details of interaction between TNP-2198 nitroimidazole pharmacophore and DNA bases. Rendering and colors as in Figure 6.

and *gyrA* genes of resistant variants were sequenced to identify the sequence changes responsible for resistance. The resulting strains provided derivatives of *C. difficile* ATCC BAA1382 bearing Rif-resistant ($rpoB^{Q489K}$) and/or Cipro-resistant ($gyrA^{A118S}$, $gyrA^{D71Y,\ T82A}$) alleles. Attempts to create metronidazole-resistant mutants were unsuccessful due to the apparent poor fitness of such mutants.

TNP-2198 was 64- to 500-fold more active than Rif against Rif-resistant (CB1934) and Rif-resistant/Cipro-resistant strains (CB1940 and CB1942), consistent with the intended dual-targeted activity of TNP-2198, in which activity against a Rif-resistant strain is provided by the nitroimidazole pharmacophore. TNP-2198 also was up to 32-fold more active than a 1:1 molar combination of Rif and Mtz, consistent with synergistic activity.

The synergistic effect of the rifamycin and metronidazole conjugate, as compared to the parent drug combinations, was further demonstrated in a time-kill kinetic study utilizing *H. pylori* ATCC 700824 (Figure 5). TNP-2198 exhibited substantially more rapid bactericidal activity than Rbt, Mtz, or a 1:1 molar combination of Rbt and Mtz.

TNP-2198 Mode of Action: Structural Basis of RNAP-Inhibitory Activity. A crystal structure of the *Mycobacterium tuberculosis* RNAP-promoter open complex bound to TNP-2198 was determined at 3.7 Å resolution (*Mtb* RPo-TNP-2198; Figures 6 and 7, Table 5). The crystal structure shows that the rifamycin pharmacophore of TNP-2198 binds to the RNAP Rif pocket, making the same interactions with the RNAP Rif pocket and being positioned to sterically block extension of short 2−3 nucleotide RNA products into longer products as previously observed for Rif (Figure 6).[24,26] The structure shows that the linker and the nitroimidazole moieties of TNP-2198 extend toward the RNAP active center, occupying a space that is occupied by bulk solvent in a transcription complex prior to RNA synthesis and that is occupied by RNA during RNA synthesis (Figure 6) and shows that the nitroimidazole moiety directly contacts template-strand single-stranded DNA at promoter positions -3 and -2, making van der Waals interactions with DNA bases at positions -3 and -2, and making a hydrogen bond with a Watson−Crick hydrogen-bonding atom of the DNA base at position -3 (Figures 6 and 7).

The interaction between the nitroimidazole moiety of TNP-2198 and template-strand single-stranded DNA likely results in higher binding affinity and higher RNAP-inhibitory activity for TNP-2198 than for Rif and potentially could result in covalent cross-linking between RNAP-bound TNP-2198 and promoter DNA, and irreversible inhibition, upon intramicrobial reductive activation of the TNP-2198 nitroimidazole moiety.

In the presence of nitroreductases, such as those present intracellularly in microaerophilically or anaerobically growing bacteria, nitroimidazoles, including metronidazole, can undergo reductive activation and can engage in covalent cross-linking with DNA bases and proteins.[29−31] The covalent cross-linking with DNA bases is thought to involve a four-electron reduction of the nitroimidazole pharmacophore, resulting in formation of a hydroxylamine-imidazole electrophile, followed by reaction with a nucleophile on a DNA base. The fact that nitroimidazoles can form covalent cross-links with DNA bases upon reductive activation in microaerophilically or anaerobically growing bacteria, together with our crystal structure showing that the nitroimidazole pharmacophore of TNP-2198 directly contacts DNA bases in RNAP-TNP-2198-promoter complex (Figures 6 and 7), raises the possibility that the nitroimidazole pharmacophore of TNP-2198 may form covalent cross-links with DNA upon reductive activation of

https://doi.org/10.1021/acs.jmedchem.1c02045
J. Med. Chem. 2022, 65, 4481−4495

the nitroimidazole pharmacophore in microaerophilically or anaerobically growing bacteria. Formation of covalent cross-links between TNP-2198 and promoter DNA would result in irreversible stabilization of the RNAP-TNP-2198-promoter complex and in irreversible inactivation of the promoter, leading to high RNAP-inhibitory activity and potentially explaining the unexpectedly high antibacterial activities, particularly the unexpectedly high antibacterial activities against Rif-resistant and Mtz-resistant strains, observed in this work (Tables 3 and 4, Figure 5). According to this hypothesis, TNP-2198 not only would exhibit dual targeting, with rifamycin pharmacophore and nitroimidazole pharmacophore activities, but also would exhibit a synergistically enhanced rifamycin pharmacophore activity, making TNP-2198 a first representative of a class of rifamycins that exhibit irreversible RNAP-inactivating and promoter-inactivating activities.

Table 4. MICs (μg/mL) of TNP-2198 against the Rif-Resistant, Cipro-Resistant, and Rif-Resistant/Cipro-Resistant *C. difficile* Strains

strain	description	Rif	Mtz	Rif + Mtz (1:1 molar ratio)	TNP-2198
CB1921	wild-type (ATCC# BAA1382)	≤0.03	0.25	≤0.03	≤0.002
CB1934	Rif-R ($rpoB^{Q489K}$)	>32	0.25	2	0.5
CB1939	FQ-R (unknown mutation)	≤0.03	0.25	≤0.03	≤0.002
CB1941	FQ-R ($gyrA^{D71Y,T82A}$)	≤0.03	0.25	≤0.03	≤0.002
CB1940	Rif-R/FQ-R ($rpoB^{Q489K}$ $gyrA^{A118S}$)	>32	0.25	2	0.5
CB1942	Rif-R/FQ-R ($rpoB^{Q489K}$ $gyrA^{D71Y, T82A}$)	>32	0.25	2	0.06

Future work on the mode of action of TNP-2198 will include determining whether covalent cross-linking between TNP-2198 and promoter DNA occurs and, if so, determining the structure and properties of the cross-linked product and defining the promoter-DNA-sequence dependences of the cross-linking reaction.

TNP-2198 *In Vitro* Antibacterial Profile. TNP-2198 was profiled for activity *in vitro* against a panel of microaerophilic and anaerobic bacteria (Table 6). TNP-2198 exhibited potent activity against microaerophilic and obligate anaerobic organisms, including those resistant to its parental rifamycin and/or nitroimidazole pharmacophores as previously discussed.

TNP-2198 was further evaluated against contemporary clinical isolates of *H. pylori*, *C. difficile*, and *G. vaginalis*, from patients in the United States and China (Table 7). TNP-2198 was more potent than rifampin, particularly against rifampin-resistant strains, with MIC_{90} values <1 μg/mL against all the clinical isolates isolated from the USA and China. TNP-2198 was significantly more potent than metronidazole, one of the drugs used as a standard-of-care therapy in the treatment of *H. pylori* and *G. vaginalis* infections.

TNP-2198 Frequency of Resistance. Based on the MIC data, TNP-2198 appears to exhibit a dual mechanism of action against microaerophilic and anaerobic bacteria and therefore would likely possess a lower propensity for the development of intrinsic resistance compared to its parent rifamycin and nitroimidazole pharmacophores. The spontaneous frequencies of resistance to TNP-2198 were measured against *H. pylori*, *C. difficile*, and *G. vaginalis* (Table 8). No drug-resistant colonies were identified at all concentrations tested for *H. pylori* MMX 3719 and *G. vaginalis* MMX 5973. The spontaneous frequencies of mutation for these two strains were $<5 \times 10^{-9}$ μg/mL and $<2 \times 10^{-9}$ μg/mL, and the mutation prevention concentrations (MPCs)[42] were ≤0.5 μg/mL and ≤0.5 μg/mL, respectively. For *C. difficile* MMX 4381, a single resistant colony was identified at the lowest concentration tested, indicating that the spontaneous frequency of mutation and MPC values. were 8×10^{-10} and 1 μg/mL, respectively.

Table 5. Data Collection and Refinement Statistics for Crystal Structure of *M. tuberculosis* RPo-(TNP-2198)[a]

PDB code	7RWI
data collection	
wavelength (Å)	0.97918
space group	$P2_12_12_1$
cell dimensions	
a, *b*, *c* (Å)	142.773, 160.613, 238.646
α, *β*, *γ* (°)	90, 90, 90
resolution (Å)	48.71−3.70 (3.76−3.70)
unique reflections	57,449 (5,678)
R_{merge}	0.177
R_{pim}	0.057
$I/\sigma(I)$	11.13 (1.04)
completeness (%)	97.3 (96.6)
$CC^{1/2}$	(0.787)
CC*	(0.938)
redundance	13.5 (12.8)
refinement	
resolution (Å)	48.71−3.70 (3.83−3.70)
number of atoms	24,903
R_{work}/R_{free}	0.2087/0.2446 (0.2980/0.3243)
total reflections	55,449 (5,491)
reflections used for R_{free}	1999 (197)
B factors (Å^2)	
macromolecules	167.39
ligands	138.52
RMSDs	
bond lengths (Å)	0.0228
bond angles (°)	0.765
clashscore	7.77
Ramachandran plot (%)	
favored	95.4
outliers	0.42
rotamer outliers (%)	0.19

[a]Numbers in parentheses refer to highest-resolution shell.

TNP-2198 Pharmacokinetics in Preclinical Species. The pharmacokinetic characteristics of TNP-2198 via intravenous (IV) and oral (PO) administration were assessed in C57BL/6 mice, Sprague−Dawley rats, and beagle dogs (Table 9). TNP-2198 was orally bioavailablee in all animal species tested with increased oral bioavailability of 20%, 48%, and 65% in mice, rats, and dogs, respectively. The half-lives of TNP-2198 were also increased from 0.51 h in mice, 0.94 h in rats, to 3.4 h in dogs. The volumes of distribution were also increased from small to large animals, ranging 0.90 L/kg, 1.6 L/kg, and 2.8 L/kg in mice, rats, and dogs, respectively.

https://doi.org/10.1021/acs.jmedchem.1c02045
J. Med. Chem. 2022, 65, 4481−4495

Table 6. *In Vitro* Antibacterial Activity of TNP-2198, Rif, Mtz, and Clindamycin (Cln) against Microaerophilic and Anaerobic Bacteria

strain	MIC (μg/mL)			
	TNP-2198	Mtz	Cln	Rif
Actinomyces naeslundii ATCC 1210	0.001	256	0.5	0.03
Atopobium vaginae BAA-55	0.03	128	0.008	0.25
Bacteroides fragilis (QC) ATCC 25285	0.03	1	1	0.25
Bacteroides fragilis (MTZ^R) MMX 3387	0.015	>256	2	0.25
Bacteroides thetaiotaomicron (MTZ^R) MMX 3409	0.03	2	>64	0.5
Bacteroides gracilis ATCC 33236, MMX 1270	0.5	>256	0.06	16
Bacteroides uniformis MMX 1277	0.03	>256	0.25	0.5
Bacteroides vulgatus MMX 8348	0.03	1	0.25	0.25
Bacteroides vulgatus (MTZ^R) 3490	0.03	128	64	0.25
Bacteroides ovatus (MTZ^R) MMX 3504	0.12	2	8	1
Bifidobacterium (breve) ATCC 15698	0.015	8	0.03	0.25
Bifidobacterium longum ATCC 15707	0.015	8	0.008	0.5
Clostridium sporogenes ATCC 19404	0.015	0.06	8	1
Clostridium difficile (RIF^R) MMX 3587	0.25	1	8	8
Fusobacterium nucleatum ATCC 10953	0.12	0.06	0.03	1
Fusobacterium nucleatum ATCC 25586	0.001	2	0.03	0.5
Gardnerella vaginalis ATCC 14018	0.004	4	0.06	0.5
Gardnerella vaginalis ATCC 49145	0.004	4	0.06	0.5
Mobiluncus (curtisii subsp. curtisii) ATCC 35241	0.002	2	0.06	0.004
Mobiluncus (mulieris) ATCC 35243	0.001	0.5	0.03	0.004
Peptococcus (niger) ATCC 27731	0.0005	0.5	0.03	0.004
Peptoniphilus (asaccharolyticus) ATCC 29743	0.008	0.5	4	0.004
Peptostreptococcus (magnus) ATCC 14956	0.0005	1	1	1
Peptostreptococcus anaerobius ATCC 27337	0.002	0.25	0.12	0.004
Prevotella asaccharolytica (MTZ^R) MMX 3552	0.008	1	32	0.004
Prevotella bivia ATCC 29303, MMX 5718	0.015	1	0.03	0.5
Prevotella bivia MMX 3450	0.0005	1	16	0.06
Prevotella bivia (MTZ^R) MMX 3454	0.015	0.5	0.06	0.004
Prevotella disiens MMX 3457	0.008	0.5	0.25	0.5
Prevotella disiens MMX 3446	0.015	0.5	0.12	0.12
Prevotella intermedia ATCC 25611, MMX 3002	0.0005	1	0.008	0.12
Treponema denticola ATCC 35405	0.002	0.5	0.12	0.004
Veionella parvula ATCC 17745, MMX 1272	2	2	32	4

TNP-2198 Tissue Distribution. The distribution of TNP-2198 in plasma and in various tissues of interest associated with various microaerophilic/anaerobic bacterial infections was assessed in Sprague–Dawley rats (Table 10). TNP-2198 exhibited a high level of distribution in stomach contents and tissues, significantly higher than that in the plasma at the same time point. The concentrations of TNP-2198 in the stomach contents and tissues 6 h after dosing were 28,789 ng/g and 10,596 ng/g, respectively, which are projected to be significantly higher than the MIC_{90} of TNP-2198 against *H. pylori* clinical isolates (125 ng/mL and 500 ng/mL in the USA and China, respectively). This stomach distribution results provides further support of TNP-2198 for the treatment of *H. pylori* infection.

TNP-2198 also demonstrated higher tissue distributions into sites associated with bacterial vaginosis. The concentration of TNP-2198 in vaginal secretions at 12 h after dosing was 366 ng/g, which is projected to be higher than the determined MIC_{90} against *G. vaginalis* (60 ng/mL), the key causative pathogen of bacterial vaginosis. TNP-2198 also exhibits high tissue distributions in the large intestine, gums, and ascites. These sites are relevant to *C. difficile* infection, gum disease, and intra-abdominal infections. Of note, TNP-2198 exhibited a relatively lower distribution to the brain, suggesting a low potential for impacting the central nervous system, a common toxicity observed for agents of the metronidazole class.

***In Vivo* Efficacy of TNP-2198 in Mouse *H. pylori* and Hamster *C. difficile* Infection Models.** TNP-2198 was evaluated in a mouse (C57/BL6) *H. pylori* infection model using a clinical isolate of *H. pylori*, named the Sydney strain *SS1* (*cagA*+, *vacA*+) adapted for the mouse model (Figure 8).[43] Animals were orally inoculated on three separate days with 6.40, 6.90 and 7.15 $\log_{10}$ CFU. This resulted in mean bacterial stomach titers of 6.50 $\log_{10}$ CFU at 7 days after the last inoculation (designated as day 0 to start of treatment). Animals administered the vehicle exhibited mean titers of 5.25 $\log_{10}$ CFU on day 7. Administration of 45, 15, and 5 mg/kg TNP-2198 reduced mean titers to 1.70, 1.94, and 2.89 $\log_{10}$ CFU, respectively. Mean bacterial stomach titers for animals administered triple therapy (consisting of omeprazole 1 mg/kg, clarithromycin 10 mg/kg, amoxicillin 20 mg/kg) were 1.70 $\log_{10}$ CFU on days 7, whereas those administered clarithromycin alone (10 mg/kg) exhibited mean counts of 2.85 $\log_{10}$ CFU on day 7. This study indicates that TNP-2198, as a single agent, exhibits equivalent efficacy to that of triple therapy and was equally or more efficacious than clarithromycin, the most potent drug against *H. pylori* infection in this preclinical model.

The efficacy of TNP-2198 in treatment of *C. difficile* associated disease (CDAD) was evaluated in a hamster infection model (male Golden Syrian hamsters) using *C. difficile* UNT103-1 (VA11–REA J-type strain, binary toxin negative, nonepidemic) (Figure 9). On day 1, at 24 h after infection, all animals received a single subcutaneous injection of clindamycin (10 mg/kg). TNP-2198 (5, 15, and 45 mg/kg) and comparators vancomycin (Vanc, 20 mg/kg) and metronidazole (100 mg/kg) were administered once-a-day (QD), starting on day 2 after clindamycin injection, for 5 consecutive days (days 2–6 via oral gavage). Animals were monitored, and a survival census was taken through day 21. Infected animals administered vehicle alone exhibited 0% survival by day 3. Animals in the groups administered 45 and 15 mg/kg of TNP-2198 exhibited 100% survival through the end of the study on day 21. Animals in the 5 mg/kg of TNP-2198 dose group exhibited 100% survival during the 5-day dosing regimen followed by 10–30% mortality from days 7–9. Metronidazole (100 mg/kg) did not provide for protection of infected animals with 100% mortality observed by day 4. Vancomycin (20 mg/kg) protected animals during treatment and through day 17 and 80% survival at the end of the study.

https://doi.org/10.1021/acs.jmedchem.1c02045
J. Med. Chem. 2022, 65, 4481–4495

Table 7. *In Vitro* Antibacterial Activity of TNP-2198, Rif, and Mtz against *H. pylori*, *C. difficile* and *G. vaginalis* Contemporary Clinical Isolates from US and China

isolates		TNP-2198		Rif		Mtz	
		MIC range (μg/mL)	MIC_{90} (μg/mL)	MIC range (μg/mL)	MIC_{90} (μg/mL)	MIC range (μg/mL)	MIC_{90} (μg/mL)
H. pylori	USA (N = 200)	≤0.001−2	0.125	0.007−≥32	2	0.25−256	128
	China (N = 49)	≤0.002−1	0.5	≤0.06−64	0.5	0.25−≥16	≥16
C. difficile	USA (N = 50)	≤0.002−4	1	NT	NT	0.12−4	1
	China (N = 46)	≤0.06−2	1	≤0.06−≥128	≥128	≤0.06−32	0.125
G. vaginalis	USA (N = 101)	≤0.004−0.06	0.06	NT	NT	2−≥64	64
	China (N = 24)	≤0.004−0.06	0.06	NT	NT	16−≥32	≥32

Table 8. Spontaneous Resistance Frequency and Mutation Prevention Concentration of TNP-2198 in *H. pylori*, *C. difficile*, and *G. vaginosis*

strain	conc. (μg/mL)	inoculum (CFU)	resistant colonies identified			spontaneous resistance frequency	MPC (μg/mL)
			test 1	test 2	mean		
H. pylori MMX 3719	0.5	1.90×10^8	0	0	0	$<5 \times 10^{-9}$	≤0.5
	1	1.90×10^8	0	0	0	$<5 \times 10^{-9}$	
	2	1.90×10^8	0	0	0	$<5 \times 10^{-9}$	
	4	1.90×10^8	0	0	0	$<5 \times 10^{-9}$	
C. difficile MMX 4381	0.5	1.23×10^9	0	1	1	8×10^{-10}	1
	1	1.23×10^9	0	0	0	$<8 \times 10^{-10}$	
	2	1.23×10^9	0	0	0	$<8 \times 10^{-10}$	
	4	1.23×10^9	0	0	0	$<8 \times 10^{-10}$	
G. Vaginalis MMX 5973	0.5	4.50×10^8	0	0	0	$<2 \times 10^{-9}$	≤0.5
	1	4.50×10^8	0	0	0	$<2 \times 10^{-9}$	
	2	4.50×10^8	0	0	0	$<2 \times 10^{-9}$	
	4	4.50×10^8	0	0	0	$<2.00 \times 10^{-9}$	

Table 9. Intravenous and Oral Pharmacokinetics of TNP-2198 in Mice, Rats, And Dogs

PK parameter	mice (C57BL/6)		rats (SD)		dogs (beagle)	
	IV (5 mg/kg)	PO (20 mg/kg)	IV (10 mg/kg)	PO (50 mg/kg)	IV (5 mg/kg)	PO (25 mg/kg)
T_{max} (h)	–	0.50	–	1.8	–	1.2
$T_{1/2}$ (h)	0.80	0.51	0.77	0.94	3.9	3.4
Vd_{ss} (L/kg)	0.90	–	1.6	–	2.8	–
CL (mL/min.kg)	23	–	26	–	20	–
AUC (ng·h/mL)	3763	3044	6487	15440	4530	14759
F (%)	–	20	–	48	–	65

Table 10. Tissue Distribution of TNP-2198[a]

tissue/fluid	TNP-2198 concentration (ng/g in tissues or ng/mL in plasma)				
	0.5 h	2 h	6 h	12 h	24 h
plasma	1704	2640	1437	4.33	BLOQ
vaginal secretion	4188	43,651	6241	366	54.6
vaginal tissue	2803	5898	2588	35.8	BLOQ
brain	114	392	156	BLOQ	BLOQ
ascites fluid	2620	5269	3478	84.5	BLOQ
gums	3471	6042	3658	115	65.3
stomach content	3,264,000	1,750,320	28,789	138	30.6
stomach tissue	113,268	72,540	10,596	114	14.4
large intestine content	1483	1166	84,300	2985	53.9
large intestine tissue	3800	8411	3656	31.6	7.26

[a]BLOQ: below limit of quantification.

CONCLUSIONS

There are major unmet needs in the treatment of bacterial infections caused by microaerophilic and anaerobic bacteria, including *Helicobacter pylori, Clostridioides difficile*, and *Gardnerella vaginalis*. These infections are associated with severe and common diseases, including gastric cancer, pseudomembranous colitis, and bacterial vaginosis.

As exemplified herein, TNP-2198 exhibits potent bactericidal activity against key microaerophilic and anaerobic bacterial pathogens, including *Helicobacter pylori, Clostridioides difficile,* and *Gardnerella vaginalis,* including rifamycin-resistant and nitroimidazole-resistant strains. TNP-2198 is orally bioavailable and demonstrates potent *in vivo* efficacy in established rodent models of *H. pylori* and *C. difficile* infection. Conjugation of a rifamycin pharmacophore and a nitroimidazole pharmacophore in TNP-2198 results in apparent synergistic activities, as exemplified by the greater activity than a 1:1 molar mixture of the parent rifamycin and nitroimidazole and activity against strains resistant to both rifamycins and nitroimidazoles. A crystal structure of TNP-2198 bound to a *Mycobacterium tuberculosis* RNA polymerase transcription initiation complex confirms that the rifamycin pharmacophore of TNP-2198 binds to the rifamycin binding site on RNAP and reveals that the nitroimidazole pharmacophore of TNP-2198 interacts directly with the DNA template-strand in the RNAP active-center cleft, forming a hydrogen-bond with a base of the DNA template strand.

The preclinical data presented herein support the further clinical development of TNP-2198 for the treatment of diseases caused by *Helicobacter pylori, Clostridioides difficile,*

https://doi.org/10.1021/acs.jmedchem.1c02045
J. Med. Chem. 2022, 65, 4481−4495

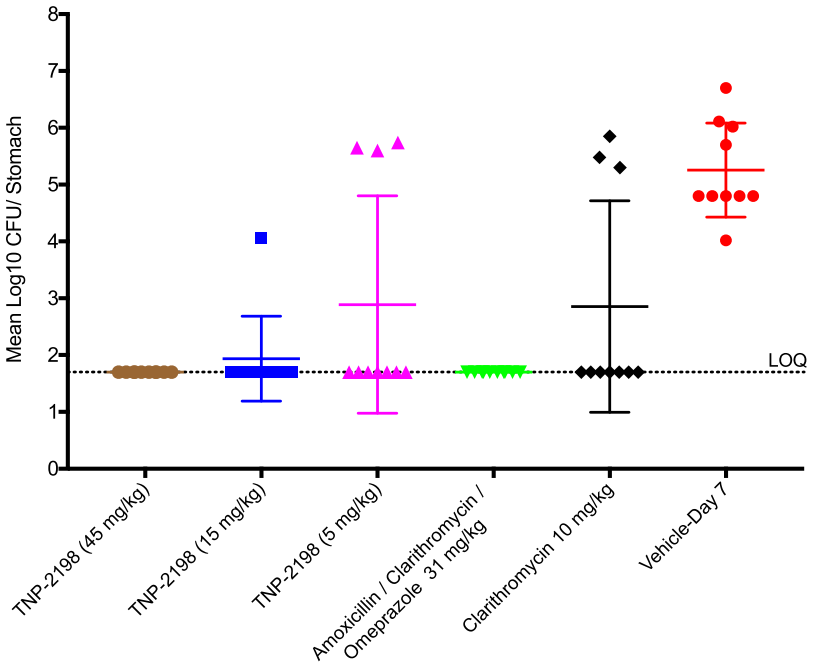

Figure 8. *In vivo* efficacy of TNP-2198, clarithromycin, and amoxicillin/clarithromycin/omeprazole in a mouse *H. pylori* infection model. Data show mean (±SD) stomach bacterial loads. LOQ: limit of quantification.

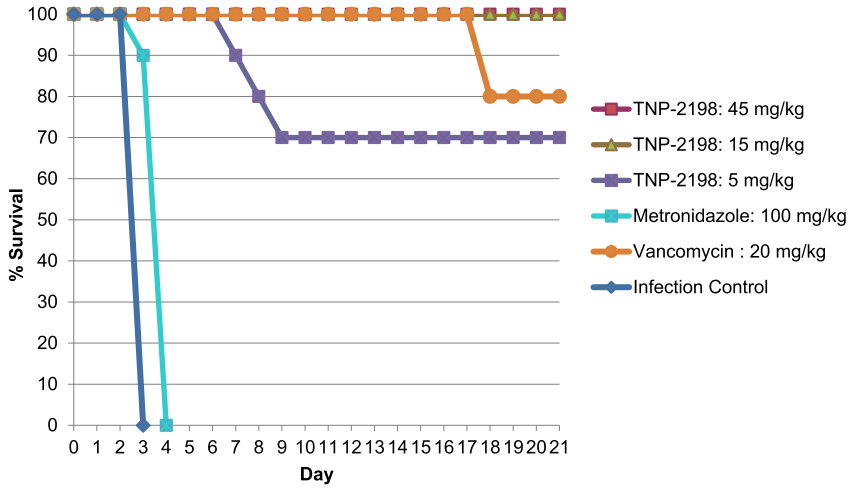

Figure 9. *In vivo* efficacy of TNP-2198, Mtz, or Vanc in a hamster *C. difficile* infection model. Data show % survival per group through 21 days.

and *Gardnerella vaginalis* and potentially other microaerophilic and anaerobic pathogens. The strategy of stably conjugating two different antimicrobial pharmacophores in a single molecular entity, as exemplified by TNP-2198 and TNP-2092,[15] provides advantages over the alternative strategy of combining two different antimicrobial agents in a combination regimen, including matched pharmacokinetics, matched tissue distribution, and, potentially, mechanism-based synergy between two pharmacophores.[20,21] Potential benefits of TNP-2198 over current therapies in the treatment of *Helicobacter pylori, Clostridioides difficile,* and *Gardnerella vaginalis* infections include a simpler regimen, reduced duration of therapy, improved safety and tolerability, activity against resistant strains, lower propensity for the emergence of resistance, and activity against contemporary clinical variants resistant to parental antibiotics. TNP-2198 is currently under clinical development for the treatment of *H. pylori* infection, *C. difficile* infection, and bacterial vaginosis.

EXPERIMENTAL METHODS

Chemistry. *General Procedures.* TNP-2198 has been prepared in milligram to kilogram quantities to support both preclinical and clinical studies. The following procedure reproduced from an issued patent is a derivation of the procedures used for manufacturing of small quantities of TNP-2198. All starting materials used were either purchased from commercial sources or prepared according to published methods. Operations involving moisture and/or oxygen sensitive materials were conducted under an atmosphere of nitrogen. Flash chromatography was performed using C60 silica gel as the normal phase adsorbent or C18 silica gel as the reverse phase adsorbent. Thin-layer chromatography and preparative thin-layer chromatography were performed using precoated plates purchased from Merck KGaA (Darmstadt, Germany), and spots were visualized with ultraviolet light followed by an appropriate staining reagent. Nuclear magnetic resonance (NMR) spectra were recorded on a Varian 400 MHz magnetic resonance spectrometer. ^{1}H NMR chemical shifts are given in parts per million (δ) downfield from TMS using the residual solvent signal ($CHCl_3$ = δ 7.27, CH_3OH = δ

https://doi.org/10.1021/acs.jmedchem.1c02045
J. Med. Chem. 2022, 65, 4481−4495

3.31) as internal standard. ^{1}H NMR information is tabulated in the following format: number of protons, multiplicity (s, singlet; d, doublet; t, triplet; q, quartet; m, multiplet; td, triplet of doublet; dt, doublet of triplet), coupling constant(s) (J) in hertz. The prefix app is occasionally applied in cases where the true signal multiplicity was not resolved, and prefix br indicates a broad signal. Electrospray ionization mass spectra were recorded on a Finnegan LCQ advantage spectrometer. High-performance liquid chromatography (HPLC) analysis for the final compound was performed on an Agilent 1100 instrument using a Waters Xterra RP18 column (5 μm, 4.6 mm × 250 mm) and gradient elution (solvent A, 20 mM NaH_2PO_4/acetonitrile, 60:40 v/v; solvent B, acetonitrile). HPLC purities for the final compound were ≥ 95%.

Synthesis of TNP-2198. Preparation of (2-Methyl-5-nitro-imidazol-1-yl)-acetaldehyde (hydrate). A solution of 2 M oxalyl chloride in CH_2Cl_2 (35 mL) was added slowly to a stirred solution of anhydrous DMSO (51 mL, 719 mmol) in CH_2Cl_2 (350 mL) at −78 °C. The resulting solution was stirred at −78 °C for 20 min. A solution of 1-hydroxyethyl-2-methyl-5-nitroimidazole (metronidazole, 10 g, 58 mmol) in DMSO (50 mL) and CH_2Cl_2 (100 mL) was added to the reaction mixture and allowed to stir for 1 h at −78 °C. Triethylamine (100 mL, 719 mmol) was then added to the solution and allowed to stir for another hour at −78 °C before the temperature of the reaction mixture was allowed to rise to room temperature. HPLC-grade water (200 mL) was added to the reaction mixture, and the resulting mixture was extracted with CH_2Cl_2 (3 × 300 mL). The combined organic layer was then dried over anhydrous Na_2SO_4, filtered, and evaporated *in vacuo*. The residue was then purified by silica gel column chromatography (3% MeOH in CH_2Cl_2) to yield the crude title compound (10.5 g) without further separation. ^{1}H NMR (400 MHz, $CDCl_3$) δ9.75 (s, 1H), 7.98 (s, 1H), 5.22 (s, 2H), 2.51 (s, 3H).

Preparation of 1-[2-(2-Methyl-5-nitro-imidazol-1-yl)-ethyl]-piperidin-4-ol. To a stirred solution of (2-methyl-5-nitro-imidazol-1-yl)-acetaldehyde (5.1 g) in CH_2Cl_2 was added 4-hydroxypiperidine (6.1 g, 60.4 mmol) and acetic acid (3.5 mL, 61 mmol), and the resulting solution allowed to stir at room temperature for 1 h. The reaction mixture was diluted with CH_2Cl_2 (20 mL) and methanol (10 mL), followed by the addition of $NaBH(OAc)_3$ (12.8 g, 60.4 mmol), and the reaction mixture allowed to stir overnight at room temperature. The reaction mixture was diluted with water (100 mL) and cooled to 0 °C. The mixture was basified to pH > 12 by adding the pellets of NaOH. The mixture was then extracted with 20% isopropyl alcohol in CH_2Cl_2 (200 mL). The combined organic layer was dried over anhydrous Na_2SO_4, filtered, and evaporated. The residue was purified by silica gel column chromatography (10% MeOH in CH_2Cl_2) to give the title product (3.2 g, 42%). ^{1}H NMR (400 MHz, $CDCl_3$) δ 7.93 (s, 1H), 4.38 (t, J = 6.4 Hz, 2H), 3.70 (m, 1H), 2.75−2.70 (m, 4H), 2.65 (t, J = 6.4 Hz, 2H), 2.51 (s, 3H), 2.25 (br t, J = 10.0 Hz, 4H).

Preparation of 1-[2-(2-Methyl-5-nitro-imidazol-1-yl)-ethyl]-piperidin-4-one. To a stirred solution of anhydrous DMSO (0.85 mL, 12 mmol) in CH_2Cl_2 (15 mL) was added 2 M oxalyl chloride in CH_2Cl_2 (3 mL) at −78 °C. The resulting solution was allowed to stir for 20 min at −78 °C. 1-[2-(2-Methyl-5-nitro-imidazol-1-yl)-ethyl]-piperidin-4-ol (1 g, 4 mmol) in CH_2Cl_2 (15 mL) was added and allowed to stir at −78 °C for 1 h. Triethylamine (5.6 mL, 40 mmol) was added and allowed to stir at −78 °C for 1 h before warming to room temperature. HPLC-grade water (20 mL) was added to the reaction mixture which was then extracted with CH_2Cl_2 (3 × 100 mL). The combined organic layer was then dried over anhydrous Na_2SO_4, filtered, and evaporated. The residue was then purified by silica gel column chromatography (6% MeOH in CH_2Cl_2) to give the title compound (481 mg, 48%). ^{1}H NMR (400 MHz, $CDCl_3$) δ 7.95 (s, 1H), 4.46 (t, J = 6.4 Hz, 2H), 2.81−2.77 (m, 6H), 2.54 (s, 3H), 2.41 (t, J = 6.4 Hz, 4H).

Preparation of 4-Deoxy-3,4-[2-spiro-[1-[2-(2-methyl-5-nitro-imidazol-1-yl)ethyl]-piperidin-4-yl]]-(1H)-imidazo-(2,5-dihydro)-rifamycin S (TNP-2198). To a stirred solution of 1-[2-(2-methyl-5-nitro-imidazol-1-yl)-ethyl]-piperidin-4-one (2.7 g, 10.7 mmol) in THF (70 mL) was added 3-amino-4-deoxy-4-imino-rifamycin S (14 g, 19.7 mmol) prepared by following a literature report.[44] Ammonium acetate (3 g, 39 mmol) was added to the reaction mixture which was allowed to stir at room temperature for 4 h. The reaction mixture was diluted with ethyl acetate and washed with water and saturated brine. The organic layer was dried over anhydrous Na_2SO_4, filtered, and evaporated. The residue was purified by silica gel column chromatography (7% MeOH in CH_2Cl_2) to give the title product (1.2 g, 12%) as dark purple solid. ESI MS m/z 944 $(M + H)^+$; HRMS (ESI): m/z $(M + H)^+$ calcd for $C_{48}H_{61}N_7O_{13}$: 944.4406, found 944.4382; ^{1}H NMR (400 MHz, $CDCl_3$) δ 14.64 (s, 1H), 8.89 (s, 1H), 8.24 (s, 1H), 7.97 (s, 1H), 6.37 (dd, J = 10.4 and 15.6 Hz, 1H), 6.27 (d, J = 10.4 Hz, 1H), 6.16 (d, J = 12.8 Hz, 1H), 6.01 (dd, J = 15.6 and 6.4 Hz, 1H), 5.12 (dd, J = 12.4 and 7.2 Hz, 1H), 4.75 (d, J = 9.2 Hz, 1H), 4.51 (br s, 1H), 4.06 (t, J = 6.8 Hz, 1H), 3.68−3.62 (m, 3H), 3.48 (s, 1H), 3.35−3.32 (m, 1H), 3.08 (s, 3H), 3.08−2.91 (m, 5H), 2.57 (s, 3H), 2.41−2.33 (m, 1H), 2.33 (s, 3H), 2.09−1.53 (m, 6H), 2.04 (s, 3H), 2.01 (s, 3H), 1.74 (s, 3H), 1.45−1.35 (m, 2H), 1.03 (d, J = 6.8 Hz, 3H), 0.84 (d, J = 7.2 Hz, 3H), 0.60 (d, J = 6.4 Hz, 3H), −0.09 (d, J = 6.8 Hz, 3H). Elemental Analysis: calcd for $C_{48}H_{61}N_7O_{13}$: C, 61.07%; H, 6.51%; N, 10.39%; O, 22.03%. Found: C, 59.18%; H, 6.72%; N, 9.98%; O, 22.24%.

***In Vitro* Microbiology.** *General Procedures.* MICs were determined for *S. aureus, H. pylori*, and *C. difficile* in accordance with contemporary Clinical and Laboratory Standards Institute (CLSI) Guidelines: (1) M7-A7 (Methods for Dilution Antimicrobial Susceptibility Tests for Bacteria That Grow Aerobically; Approved Standard) and (2) M11-A6 (Methods for Antimicrobial Susceptibility Testing of Anaerobic Bacteria; Approved Standard). Time-kill kinetic studies were similarly undertaken in accordance with the CLSI Guidance M26-A: Methods for Determining Bactericidal Activity of Antimicrobial Agents; Approved Guideline.

Strain Construction. Single-step selections of antibiotic-resistant mutants were undertaken by standard agar-based methods. Selection of rifamycin resistance employed rifampin; selection of quinolone resistance employed ciprofloxacin; and selection of nitroimidazole resistance employed metronidazole. In some cases, a second round of selection on each respective antibiotic containing plate was undertaken to increase the level of drug resistance. For *H. pylori*, combinations of mutations conferring drug resistance to more than one class of antibiotic were generated by natural transformation of PCR amplified target alleles encompassing the resistance determining regions of an individual targeted gene.[45] In all cases, mutants were purified through drug-free passage, and the initial antibiotic resistance phenotype was then verified to ensure that stable, true-breeding mutants had been obtained. Genotypic analysis of strains exhibiting stable resistance phenotypes was undertaken by standard methods with amplification and DNA sequencing of the target loci.

Antimicrobial Testing against H. pylori-Resistant Mutant Panels In Vitro. H. pylori ATCC #700392 (CB1531) is a wild-type strain originally purchased from the American Type Culture Collection (ATCC, Manassas, VA). CB1573, CB1612, CB1613, CB1614, CB1771, CB1893, CB1902, and CB1903 are derivatives of CB1531 carrying defined drug resistance determinants. All strains were provided by TenNor Therapeutics. MIC testing was performed using the agar dilution technique in accordance with CLSI approved methods.[46] Antimicrobials were prepared from 100× stocks as 2-fold dilutions in Mueller−Hinton agar with aged (≥2 weeks old) sheep blood (5% v/v). *H. pylori* MIC values were determined after 5 days incubation at 35 °C in a microaerobic growth environment produced by a gas-generating system suitable for campylobacters. For routine cultivation of *H. pylori*, trypticase soy agar with 5% sheep's blood (TSAII) was used.

Antimicrobial Testing against C. difficile-Resistant Mutant Panels In Vitro. C. difficile ATCC #BAA-1382 (CB1921) is a toxigenic strain (*tcdA*$^+$, *tcdAB*$^+$) originally purchased from the American Type Culture Collection (ATCC, Manassas, VA). CB1934, CB1939, CB1940, CB1941, and CB1942 are strains derived from CB1921 carrying defined drug resistance determinants. Antimicrobials were prepared from 100× stocks as 2-fold dilutions

https://doi.org/10.1021/acs.jmedchem.1c02045
J. Med. Chem. 2022, 65, 4481−4495

in supplemented brucella agar (brucella broth base, agar, 10 mg/L vitamin K1, 5 mg/L hemin, 5% (w/v) laked sheep's blood). *C. difficile* MIC values were determined after 3 days incubation at 35 °C under anaerobic conditions produced by gas-generating systems in closed chambers with a methylene blue indicator.

***In Vivo* Microbiology.** All *in vivo* experiments were performed in compliance with the appropriate laws and institutional guidelines. The following studies were performed at University of Northern Texas Health Science Center by following the Institutional Animal Care and Use Committee (IACUC) approved protocols, which were developed and validated from the literature and other reported methods.

H. pylori Infection Model. *H. pylori* SS1 ($CagA^+$, $VacA^+$) was adapted for mice from a human clinical isolate and has been validated in mice *H. plyori* infection models.[47] Bacteria were incubated on Columbia 3.5% laked horse blood agar plates for 5 days, plates were then scraped, and the plate scrapings suspended in sterile 0.9% saline to an OD_{530} of 1.5−2.0 to yield bacterial suspensions, and serially dilutions were plated on Columbia 3.5% laked horse blood agar plates for CFU counting. Male C57/BL6, 20−25 g mice (Charles River Laboratories, housed 1 per cage with free access to food and water in accordance with NIH and local IACUC guidelines) were inoculated orally with 0.25 mL of bacterial stock suspension on successive days using a 20−22 G gavage needle. Starting 7 days after the final inoculation, and continuing for 7 days, test compound (TNP-2198), positive control compounds, or negative control (vehicle only) were administered twice per day (bid) by oral gavage. Mice were euthanized ∼18−20 h after the last dose and 18 h after the last access to food. Stomachs were removed by cutting the esophagus away from the superior aspect of the stomach and the duodenum away from the pyloric region, rinsed in sterile PBS, homogenized, and diluted in PBS then spot plated onto Columbia agar with 7% laked horse blood ± the *H. pylori* selective supplement (Dent). Plates were incubated microaerobically at 37 °C, and colony forming unit (CFU) counts determined after 6−7 days of incubation. The LOQ was defined as < 2.35 $\log_{10}$ CFU per stomach.

C. difficile Infection Model. This model employed *C. difficile* strain UNT103-1 (VA11)—a nonepidemic ($cdtB^-$), restriction endonuclease analysis [REA] J-type strain—a clinical isolate received from Curtis Donskey (Cleveland VA Hospital, Cleveland, OH) and was previously utilized in the hamster model.[47] A bacterial culture in sporulation medium (SM) broth was diluted to OD_{600nm} = 1 (∼1.0×10^9 CFU/mL) in prereduced SM broth to yield a bacterial suspension, and serially dilutions of the bacterial suspension in prereduced tryptone glucose yeast extract broth were plated on TSA + SB (5%) agar for CFU counting. Male 80−90 g Golden Syrian hamsters (Charles River Laboratories, housed 1 per cage with free access to food and water in accordance with NIH and IACUC guidelines) were inoculated orally using a 20−22 G gavage needle and, in parallel, plated on TSA + SB (5%) agar for CFU counting as serial dilutions. One day after the third inoculation, all mice received a single subcutaneous injection of 10 mg/kg clindamycin. Starting 18 h after administration of clindamycin, and continuing for 5 days, test compound (TNP-2198), and positive-control compounds (vancomycin and metronidazole), and negative controls (vehicle) were administered once per day (QD) by oral gavage. Animals were monitored, and a survival census was taken through day 21.

Crystal Structure Determination. Crystals of *M. tuberculosis* σ^L RPo (prepared per ref 48 were soaked overnight at 22 °C in 1 mM TNP-2198 in 100 mM sodium citrate, pH 5.6, 200 mM sodium acetate, 10% (m/v) PEG-4000, 20% (v/v) (2*R*,3*R*)-(−)-2,3-butanediol, and were flash-frozen in liquid nitrogen.

X-ray diffraction data were collected at the Stanford Synchrotron Radiation Lightsource (SSRL) beamline 12-2 and were processed using HKL2000.[49] The structure was solved by molecular replacement using the structure of *M. tuberculosis* σ^L RPo (PDB 6DVC)[26] as the search model. Cycles of model building and refinement were performed using Coot[50] and Phenix Refine.[51] The final model was obtained by a refinement using secondary-structure restraints and individual and group B-factors. The atomic model and structure factors were deposited in the Protein Data Bank (PDB) with accession code 7RWI.

■ ASSOCIATED CONTENT

Supporting Information

The Supporting Information is available free of charge at https://pubs.acs.org/doi/10.1021/acs.jmedchem.1c02045.

^{1}H NMR, ^{13}C NMR, HRMS, IR, and UV spectra and HPLC trace for TNP-2198, HPLC traces for compounds **1**, **10**, **12**, and **13** (PDF)

molecular formula strings and biological data for selected compounds (CSV)

Mycobacterium tuberculosis RNA polymerase sigma L holoenzyme open promoter complex containing TNP-2198 (PDB ID: 7RWI) (PDB)

■ AUTHOR INFORMATION

Corresponding Author

Zhenkun Ma − *TenNor Therapeutics Ltd, Suzhou 215123, China*; orcid.org/0000-0002-7294-329X; Phone: +86 512-8686-1980; Email: zhenkun.ma@tennorx.com

Authors

Shijie He − *TenNor Therapeutics Ltd, Suzhou 215123, China*

Ying Yuan − *TenNor Therapeutics Ltd, Suzhou 215123, China*

Zhijun Zhuang − *TenNor Therapeutics Ltd, Suzhou 215123, China*

Yu Liu − *TenNor Therapeutics Ltd, Suzhou 215123, China*

Huan Wang − *TenNor Therapeutics Ltd, Suzhou 215123, China*

Jing Chen − *TenNor Therapeutics Ltd, Suzhou 215123, China*

Xiangyi Xu − *TenNor Therapeutics Ltd, Suzhou 215123, China*

Charles Ding − *TenNor Therapeutics Ltd, Suzhou 215123, China*; Present Address: WuXi AppTec. Co. Ltd., Shanghai 200131, China

Vadim Molodtsov − *Waksman Institute and Department of Chemistry and Chemical Biology, Rutgers University, Piscataway, New Jersey 08854, United States*

Wei Lin − *Waksman Institute and Department of Chemistry and Chemical Biology, Rutgers University, Piscataway, New Jersey 08854, United States*; Present Address: Department of Microbiology and Immunology, Nanjing University of Chinese Medicine, Nanjing, Jiangsu 210023, China; orcid.org/0000-0002-2940-6966

Gregory T. Robertson − *Department of Microbiology, Immunology and Pathology, Colorado State University, Fort Collins, Colorado 80523-1682, United States*

William J. Weiss − *HSC College of Pharmacy, University of North Texas, Fort Worth, Texas 76107, United States*

Mark Pulse − *HSC College of Pharmacy, University of North Texas, Fort Worth, Texas 76107, United States*

Phung Nguyen − *HSC College of Pharmacy, University of North Texas, Fort Worth, Texas 76107, United States*

Leonard Duncan − *JMI Laboratories, North Liberty, Iowa 52317, United States*

Timothy Doyle − *JMI Laboratories, North Liberty, Iowa 52317, United States*

Richard H. Ebright − *Waksman Institute and Department of Chemistry and Chemical Biology, Rutgers University, Piscataway, New Jersey 08854, United States*

Anthony Simon Lynch − *TenNor Therapeutics Ltd, Suzhou 215123, China*

Complete contact information is available at: https://pubs.acs.org/10.1021/acs.jmedchem.1c02045

Notes

The authors declare the following competing financial interest(s): Z.M., S.H., Y.Y., Z.Z., Y.L., H.W., J.C., and X.X. are employees and A.S.L. is a consultant of TenNor Therapeutics currently developing TNP-2198.

■ ACKNOWLEDGMENTS

The authors would like to thank the National Science and Technology Project of China (grant no. 2019ZX09721-001-004-008) for partial financial support of the work presented in this manuscript. For structural biology studies reported herein, we thank the Stanford Synchrotron Radiation Lightsource for beamline access. The structural biology work was supported by National Institutes of Health grant GM041376 to R.H.E. The authors thank current and past colleagues, academic collaborators, and supporting Contract Research Organizations for their respective contributions.

■ ABBREVIATIONS USED

AMR, antimicrobial resistance; ATCC, American Type Culture Collection; AUC, area under the curve; BLOQ, below limit of quantification; CDAD, *Clostridioides difficile*-associated diarrhea; CFU, colony forming unit; CL, clearance; Cln, clindamycin; CLSI, clinical and laboratory standards institute; CRAB, carbapenem-resistant *Acinetobacter baumannii*; CRE, carbapenem-resistant Enterobacteriaceae; Del, delamanid; DMSO, dimethyl sulfoxide; DNA, deoxyribonucleic acid; FQ, fluoroquinolone; HIV, human immunodeficiency virus; HPLC, high-performance liquid chromatography; IACUC, Institutional Animal Care and Use Committee; IR, infrared; IV, intravenous; LOQ, limit of quantitation; MALT, mucosa-associated lymphoid tissue; MIC, minimum inhibitory concentration; MPC, mutation prevention concentration; MRSA, methicillin-resistant *Staphylococcus aureus*; HRMS, high-resolution mass spectrometry; Mtz, metronidazole; NMR, nuclear magnetic resonance; NT, not tested; PCR, polymerase chain reaction; PDB, Protein Data Bank; PEG, polyethylene glycol; PK, pharmacokinetics; PO, oral; *p*-Ph, *para*-phenylene; Pre, pretomanid; Pz, piperazine-1,4-diyl; QD, once a day; Rbt, rifabutin; REA, restriction endonuclease analysis; Rfz, rifalazil; Rif, rifampin; RMSD, root-mean-square deviation; RNA, ribonucleic acid; RNAP, RNA polymerase; Rxm, rifaximin; SAR, structure−activity relationship; SD, standard deviation; SM, sporulation medium; SSRL, Stanford Synchrotron Radiation Light source; T_{max}, time to maximal concentration; $T_{1/2}$, half-time; TSA, trypticase soy agar; Vanc, vancomycin; Vd_{SS}, apparent volume of distribution at steady state

■ REFERENCES

(1) World Health Organization. *Global shortage of innovative antibiotics fuels emergence and spread of drug-resistance*; WHO: Geneva, 2021. https://www.who.int/news/item/15-04-2021-global-shortage-of-innovative-antibiotics-fuels-emergence-and-spread-of-drug-resistance (accessed 2022-01-12).

(2) U.S. Department of Health and Human Services, CDC. *Antibiotic resistance threats in the United States*; CDC: Atlanta, GA, 2019.

(3) The Pew Charitable Trusts. *Tracking the global pipeline of antibiotics in development*; The Pew Charitable Trusts: Philadelphia, PA, 2021. https://www.pewtrusts.org/en/research-and-analysis/issue-briefs/2019/03/tracking-the-global-pipeline-of-antibiotics-in-development (accessed 2022-01-12).

(4) Roszczenko-Jasińska, P.; Wojtyś, M. I.; Jagusztyn-Krynicka, E. K. Helicobacter pylori treatment in the post-antibiotics era-searching for new drug targets. *Appl. Microbiol. Biotechnol.* **2020**, *104* (23), 9891−9905.

(5) Singh, S. P.; Ahuja, V.; Ghoshal, U. C.; Makharia, G.; Dutta, U.; Zargar, S. A.; Venkataraman, J.; Dutta, A. K.; Mukhopadhyay, A. K.; Singh, A.; Thapa, B. R.; Vaiphei, K.; Sathiyasekaran, M.; Sahu, M. K.; Rout, N.; Abraham, P.; Dalai, P. C.; Rathi, P.; Sinha, S. K.; Bhatia, S.; Patra, S.; Ghoshal, U.; Poddar, U.; Mouli, V. P.; Kate, V. Management of Helicobacter pylori infection: the Bhubaneswar Consensus Report of the Indian Society of Gastroenterology. *Indian J Gastroenterol* **2021**, *40*, 420−444.

(6) Muzny, C. A.; Łaniewski, P.; Schwebke, J. R.; Herbst-Kralovetz, M. M. Host-vaginal microbiota interactions in the pathogenesis of bacterial vaginosis. *Curr Opin Infect Dis* **2020**, *33* (1), 59−65.

(7) Saleem, N.; Howden, C. W. Update on the management of Helicobacter pylori infection. *Curr Treat Options Gastroenterol* **2020**, *18*, 476−487.

(8) Tacconelli, E.; Carrara, E.; Savoldi, A.; Harbarth, S.; Mendelson, M.; Monnet, D. L.; Pulcini, C.; Kahlmeter, G.; Kluytmans, J.; Carmeli, Y.; Ouellette, M.; Outterson, K.; Patel, J.; Cavaleri, M.; Cox, E. M.; Houchens, C. R.; Grayson, M. L.; Hansen, P.; Singh, N.; Theuretzbacher, U.; Magrini, N.; et al. Discovery, research, and development of new antibiotics: the WHO priority list of antibiotic-resistant bacteria and tuberculosis. *Lancet Infect Dis* **2018**, *18* (3), 318−327.

(9) Fallone, C. A.; Chiba, N.; van Zanten, S. V.; Fischbach, L.; Gisbert, J. P.; Hunt, R. H.; Jones, N. L.; Render, C.; Leontiadis, G. I.; Moayyedi, P.; Marshall, J. K. The Toronto consensus for the treatment of Helicobacter pylori infection in adults. *Gastroenterology* **2016**, *151* (1), 51−69.e14.

(10) Fallone, C. A.; Moss, S. F.; Malfertheiner, P. Reconciliation of recent Helicobacter pylori treatment guidelines in a time of increasing resistance to antibiotics. *Gastroenterology* **2019**, *157* (1), 44−53.

(11) Savoldi, A.; Carrara, E.; Graham, D. Y.; Conti, M.; Tacconelli, E. Prevalence of antibiotic resistance in Helicobacter pylori: a systematic review and meta-analysis in World Health Organization regions. *Gastroenterology* **2018**, *155* (5), 1372−1382.e17.

(12) Zar, F. A.; Bakkanagari, S. R.; Moorthi, K. M.; Davis, M. B. A comparison of vancomycin and metronidazole for the treatment of Clostridium difficile-associated diarrhea, stratified by disease severity. *Clin Infect Dis* **2007**, *45* (3), 302−307.

(13) Gerding, D. N.; Kelly, C. P.; Rahav, G.; Lee, C.; Dubberke, E. R.; Kumar, P. N.; Yacyshyn, B.; Kao, D.; Eves, K.; Ellison, M. C.; Hanson, M. E.; Guris, D.; Dorr, M. B. Bezlotoxumab for prevention of recurrent Clostridium difficile infection in patients at increased risk for recurrence. *Clin Infect Dis* **2018**, *67* (5), 649−656.

(14) Bagnall, P.; Rizzolo, D. Bacterial vaginosis: a practical review. *Jaapa* **2017**, *30* (12), 15−21.

(15) Ma, Z.; Lynch, A. S. Development of a dual-acting antibacterial agent (TNP-2092) for the treatment of persistent bacterial infections. *J. Med. Chem.* **2016**, *59* (14), 6645−6657.

(16) Robertson, G. T.; Bonventre, E. J.; Doyle, T. B.; Du, Q.; Duncan, L.; Morris, T. W.; Roche, E. D.; Yan, D.; Lynch, A. S. In vitro evaluation of CBR-2092, a novel rifamycin-quinolone hybrid antibiotic: microbiology profiling studies with staphylococci and streptococci. *Antimicrob. Agents Chemother.* **2008**, *52* (7), 2324−2334.

(17) Robertson, G. T.; Bonventre, E. J.; Doyle, T. B.; Du, Q.; Duncan, L.; Morris, T. W.; Roche, E. D.; Yan, D.; Lynch, A. S. In vitro evaluation of CBR-2092, a novel rifamycin-quinolone hybrid antibiotic: studies of the mode of action in Staphylococcus aureus. *Antimicrob. Agents Chemother.* **2008**, *52* (7), 2313−2323.

(18) Yuan, Y.; Wang, X.; Xu, X.; Liu, Y.; Li, C.; Yang, M.; Yang, Y.; Ma, Z. Evaluation of a dual-acting antibacterial agent, TNP-2092, on

gut microbiota and potential application in the treatment of gastrointestinal and liver disorders. *ACS Infect Dis* **2020**, *6* (5), 820−831.
(19) Fisher, C. R.; Schmidt-Malan, S. M.; Ma, Z.; Yuan, Y.; He, S.; Patel, R. In vitro activity of TNP-2092 against periprosthetic joint infection-associated staphylococci. *Diagn Microbiol Infect Dis* **2020**, *97* (3), 115040.
(20) Zhuang, Z.; Wan, D.; Ding, J.; He, S.; Zhang, Q.; Wang, X.; Yuan, Y.; Lu, Y.; Ding, C. Z.; Lynch, A. S.; Upton, A. M.; Cooper, C. B.; Denny, W. A.; Ma, Z. Synergistic activity of nitroimidazole-oxazolidinone conjugates against anaerobic bacteria. *Molecules* **2020**, *25* (10), 2431.
(21) Surur, A. S.; Sun, D. Macrocycle-antibiotic hybrids: a path to clinical candidates. *Front Chem* **2021**, *9*, 659845.
(22) Aristoff, P. A.; Garcia, G. A.; Kirchhoff, P. D.; Showalter, H. D. Rifamycins–obstacles and opportunities. *Tuberculosis (Edinb)* **2010**, *90* (2), 94−118.
(23) Nazli, A.; He, D.; Xu, H.; Wang, Z. P.; He, Y. A comparative insight on the newly emerging rifamycins: rifametane, rifalazil, TNP-2092 and TNP-2198. *Curr Med Chem* **2021**, DOI: 10.2174/0929867328666210806114949.
(24) Campbell, E. A.; Korzheva, N.; Mustaev, A.; Murakami, K.; Nair, S.; Goldfarb, A.; Darst, S. A. Structural mechanism for rifampicin inhibition of bacterial rna polymerase. *Cell* **2001**, *104* (6), 901−912.
(25) Ho, M. X.; Hudson, B. P.; Das, K.; Arnold, E.; Ebright, R. H. Structures of RNA polymerase-antibiotic complexes. *Curr Opin Struct Biol* **2009**, *19* (6), 715−723.
(26) Lin, W.; Mandal, S.; Degen, D.; Liu, Y.; Ebright, Y. W.; Li, S.; Feng, Y.; Zhang, Y.; Mandal, S.; Jiang, Y.; Liu, S.; Gigliotti, M.; Talaue, M.; Connell, N.; Das, K.; Arnold, E.; Ebright, R. H. Structural basis of Mycobacterium tuberculosis transcription and transcription inhibition. *Mol. Cell* **2017**, *66* (2), 169−179.e8.
(27) Feklistov, A.; Mekler, V.; Jiang, Q.; Westblade, L. F.; Irschik, H.; Jansen, R.; Mustaev, A.; Darst, S. A.; Ebright, R. H. Rifamycins do not function by allosteric modulation of binding of Mg2+ to the RNA polymerase active center. *Proc Natl Acad Sci U S A* **2008**, *105* (39), 14820−14825.
(28) Dubbreuil, L. 5′-Nitroimadazoles. In *Antimicrobial Agents: Antibacterials and antifungals*, Bryskier, A., Ed.; ASM Press: Washington, 2005; pp 930−940.
(29) Showalter, H. D. Recent progress in the discovery and development of 2-nitroimidazooxazines and 6-nitroimidazooxazoles to treat tuberculosis and neglected tropical diseases. *Molecules* **2020**, *25* (18), 4137.
(30) Kedderis, G. L.; Argenbright, L. S.; Miwa, G. T. Covalent interaction of 5-nitroimidazoles with DNA and protein in vitro: mechanism of reductive activation. *Chem. Res. Toxicol.* **1989**, *2* (3), 146−149.
(31) Ang, C. W.; Jarrad, A. M.; Cooper, M. A.; Blaskovich, M. A. T. Nitroimidazoles: molecular fireworks that combat a broad spectrum of infectious diseases. *J. Med. Chem.* **2017**, *60* (18), 7636−7657.
(32) Molodtsov, V.; Nawarathne, I. N.; Scharf, N. T.; Kirchhoff, P. D.; Showalter, H. D.; Garcia, G. A.; Murakami, K. S. X-ray crystal structures of the Escherichia coli RNA polymerase in complex with benzoxazinorifamycins. *J. Med. Chem.* **2013**, *56* (11), 4758−4763.
(33) Molodtsov, V.; Scharf, N. T.; Stefan, M. A.; Garcia, G. A.; Murakami, K. S. Structural basis for rifamycin resistance of bacterial RNA polymerase by the three most clinically important RpoB mutations found in Mycobacterium tuberculosis. *Mol. Microbiol.* **2017**, *103* (6), 1034−1045.
(34) Mosaei, H.; Molodtsov, V.; Kepplinger, B.; Harbottle, J.; Moon, C. W.; Jeeves, R. E.; Ceccaroni, L.; Shin, Y.; Morton-Laing, S.; Marrs, E. C. L.; Wills, C.; Clegg, W.; Yuzenkova, Y.; Perry, J. D.; Bacon, J.; Errington, J.; Allenby, N. E. E.; Hall, M. J.; Murakami, K. S.; Zenkin, N. Mode of action of kanglemycin A, an ansamycin natural product that is active against rifampicin-resistant Mycobacterium tuberculosis. *Mol. Cell* **2018**, *72* (2), 263−274.e5.
(35) Artsimovitch, I.; Vassylyeva, M. N.; Svetlov, D.; Svetlov, V.; Perederina, A.; Igarashi, N.; Matsugaki, N.; Wakatsuki, S.; Tahirov, T. H.; Vassylyev, D. G. Allosteric modulation of the RNA polymerase catalytic reaction is an essential component of transcription control by rifamycins. *Cell* **2005**, *122* (3), 351−363.
(36) Peek, J.; Lilic, M.; Montiel, D.; Milshteyn, A.; Woodworth, I.; Biggins, J. B.; Ternei, M. A.; Calle, P. Y.; Danziger, M.; Warrier, T.; Saito, K.; Braffman, N.; Fay, A.; Glickman, M. S.; Darst, S. A.; Campbell, E. A.; Brady, S. F. Rifamycin congeners kanglemycins are active against rifampicin-resistant bacteria via a distinct mechanism. *Nat Commun* **2018**, *9* (1), 4147.
(37) Ebright, R. H.; Ebright, Y. W.; Lin, C. T. Antibacterial agents: dual-targeted RNA polymerase inhibitors. WO 2019226915 A1, May 25, 2018.
(38) Zhang, Y.; Degen, D.; Ho, M. X.; Sineva, E.; Ebright, K. Y.; Ebright, Y. W.; Mekler, V.; Vahedian-Movahed, H.; Feng, Y.; Yin, R.; Tuske, S.; Irschik, H.; Jansen, R.; Maffioli, S.; Donadio, S.; Arnold, E.; Ebright, R. H. GE23077 binds to the RNA polymerase 'i' and 'i+1' sites and prevents the binding of initiating nucleotides. *Elife* **2014**, *3*, No. e02450.
(39) Ding, C. Z.; Kim, I. H.; Wang, J.; Ma, Z.; Jin, Y.; Combrink, K. D.; Lu, G.; Lynch, A. S. Nitroheteroaryl-containing rifamycin derivatives. US 7678791 B2, March 16, 2010.
(40) Zhang, S.; Wang, X.; Wise, M. J.; He, Y.; Chen, H.; Liu, A.; Huang, H.; Young, S.; Tay, C. Y.; Marshall, B. J.; Li, X.; Chua, E. G. Mutations of Helicobacter pylori RdxA are mainly related to the phylogenetic origin of the strain and not to metronidazole resistance. *J. Antimicrob. Chemother.* **2020**, *75* (11), 3152−3155.
(41) Martínez-Júlvez, M.; Rojas, A. L.; Olekhnovich, I.; Espinosa Angarica, V.; Hoffman, P. S.; Sancho, J. Structure of RdxA–an oxygen-insensitive nitroreductase essential for metronidazole activation in Helicobacter pylori. *Febs j* **2012**, *279* (23), 4306−4317.
(42) Drlica, K. The mutant selection window and antimicrobial resistance. *J. Antimicrob. Chemother.* **2003**, *52* (1), 11−17.
(43) Lee, A.; O'Rourke, J.; De Ungria, M. C.; Robertson, B.; Daskalopoulos, G.; Dixon, M. F. A standardized mouse model of Helicobacter pylori infection: introducing the Sydney strain. *Gastroenterology* **1997**, *112* (4), 1386−1397.
(44) Marsili, L.; Rossetti, V.; Pasqualucci, C. Rifamycin compounds. US 4017481 A, April 12, 1977.
(45) Moore, R. A.; Beckthold, B.; Wong, S.; Kureishi, A.; Bryan, L. E. Nucleotide sequence of the gyrA gene and characterization of ciprofloxacin-resistant mutants of Helicobacter pylori. *Antimicrob. Agents Chemother.* **1995**, *39* (1), 107−111.
(46) Clinical and Laboratory Standards Institute. *Methods for Dilution Antimicrobial Susceptibility Tests for Bacteria That Grow Aerobically, M7-A7*, Approved Standard, 9 ed.; CLSI: Wayne, PA, 2018.
(47) Weiss, W.; Pulse, M.; Vickers, R. In vivo assessment of SMT19969 in a hamster model of clostridium difficile infection. *Antimicrob. Agents Chemother.* **2014**, *58* (10), 5714−5718.
(48) Li, L.; Molodtsov, V.; Lin, W.; Ebright, R. H.; Zhang, Y. RNA extension drives a stepwise displacement of an initiation-factor structural module in initial transcription. *Proc Natl Acad Sci U S A* **2020**, *117* (11), 5801−5809.
(49) Otwinowski, Z.; Minor, W. Processing of X-ray diffraction data collected in oscillation mode. *Methods Enzymol* **1997**, *276*, 307−326.
(50) Emsley, P.; Cowtan, K. Coot: model-building tools for molecular graphics. *Acta Crystallogr D Biol Crystallogr* **2004**, *60* (12), 2126−2132.
(51) Afonine, P. V.; Mustyakimov, M.; Grosse-Kunstleve, R. W.; Moriarty, N. W.; Langan, P.; Adams, P. D. Joint X-ray and neutron refinement with phenix.refine. *Acta Crystallogr D Biol Crystallogr* **2010**, *66* (11), 1153−1163.

https://doi.org/10.1021/acs.jmedchem.1c02045
J. Med. Chem. 2022, 65, 4481−4495